

Cosmological implications of gauged $U(1)_{B-L}$ on ΔN_{eff} in the CMB and BBN

Haidar Esseili and Graham D. Kribs

Department of Physics and Institute for Fundamental Science,
University of Oregon, Eugene, Oregon 97403, USA

E-mail: hesseili@uoregon.edu, kribs@uoregon.edu

Abstract. We calculate the effects of a light, very weakly-coupled boson X arising from a spontaneously broken $U(1)_{B-L}$ symmetry on ΔN_{eff} as measured by the CMB and Y_p from BBN. Our focus is the mass range $1 \text{ eV} \lesssim m_X \lesssim 100 \text{ MeV}$; masses lighter than about an eV have strong constraints from fifth-force law constraints, while masses heavier than about 100 MeV are constrained by other probes, including terrestrial experiments. We do *not* assume X began in thermal equilibrium with the SM; instead, we allow X to freeze-in from its very weak interactions with the SM. We find $U(1)_{B-L}$ is more strongly constrained by ΔN_{eff} than previously considered. The bounds arise from the energy density in electrons and neutrinos slowly siphoned off into X bosons, which become nonrelativistic, redshift as matter, and then decay, dumping their slightly larger energy density back into the SM bath causing $\Delta N_{\text{eff}} > 0$. While some of the parameter space has complementary constraints from stellar cooling, supernova emission, and terrestrial experiments, we find future CMB observatories including Simons Observatory and CMB-S4 can access regions of mass and coupling space not probed by any other method. In gauging $U(1)_{B-L}$, we assume the $[U(1)_{B-L}]^3$ anomaly is canceled by right-handed neutrinos, and so our ΔN_{eff} calculations have been carried out in two scenarios: neutrinos have Dirac masses, or, right-handed neutrinos acquire Majorana masses. In the latter scenario, we comment on the additional implications of thermalized right-handed neutrinos decaying during BBN. We also briefly consider the possibility that X decays into dark sector states. If these states behave as radiation, we find weaker constraints, whereas if they are massive, there are stronger constraints, though now from $\Delta N_{\text{eff}} < 0$.

Contents

1	Introduction	3
2	Gauged $U(1)_{B-L}$: Majorana and Dirac neutrino cases	4
2.1	Neutrino masses: Majorana and Dirac cases	5
3	Effective number of relativistic species: N_{eff}	6
4	Early universe thermodynamics	7
4.1	Approximations	8
4.2	Boltzmann equations	9
4.3	Collision terms	10
4.3.1	Electron-neutrino interactions	10
4.3.2	Decays and inverse decays	12
4.3.3	Electron-X interactions	13
4.3.4	Suppressed interactions	14
4.4	Summary of transfer rates	14
5	Numerical evolution of the Boltzmann equations and N_{eff}	14
5.1	Initial conditions	14
5.2	Evolution of Boltzmann equations	15
5.3	Numerical results for N_{eff}	17
5.4	Other constraints	22
5.5	Constraints from existing CMB observations and prospects for future observatories	23
6	Semi-analytic estimates of delta ΔN_{eff}	24
6.1	Majorana case	25
6.2	Dirac and generalized cases	26
6.2.1	Dirac case	26
6.2.2	Large number of massless species	27
6.2.3	Massive species	27
7	BBN Y_p	27
8	Discussion	29
A	Right-handed neutrino decay in Majorana case	32
B	Finite Temperature Effects	33
B.1	$m_\gamma(T) \ll m_X$	34
B.2	$m_\gamma(T) \gg m_X$	35
B.3	$m_\gamma(T) = m_X$ resonance	35
B.4	Implications of the resonance on our results	36

1 Introduction

Light mediators – new massive, unstable particles that couple to the SM – have seen tremendous interest over the past decade (for reviews, see [1, 2]). They are essential to models of light dark matter [3–5], providing mechanisms that lead to the correct abundance as well as providing detectable signals in the myriad landscape of light dark matter detection experiments. A panoply of experiments have been considered to gain sensitivity to these mediators.

Specializing to light $U(1)$ vector boson mediators, several varieties have been considered: the dark photon (for a recent review, see [6]); $U(1)_{B-L}$ (early discussions include [7–10] and a review of massive Z 's [11]), while gauged $U(1)_{B-L}$ as a light mediator has been considered in detail in [12–15]; $U(1)_B$ [16–18]; and flavor-dependent $U(1)$ s such as $U(1)_{\mu-\tau}$ [19–21] (some recent work [22, 23]). A huge variety of constraints restrict the parameter space of these light vector bosons [12–15, 24] including colliders, fixed target experiments, energy loss from stars; energy loss from supernovae, changes to big-bang nucleosynthesis; etc.

Our focus in this paper is to calculate the contributions to the effective number of relativistic species, N_{eff} , from a light $U(1)_{B-L}$ gauge boson mediator X , determining both the existing constraints and prospects for future CMB observatories. Precision determination of N_{eff} , from CMB power spectra [25, 26] and primordial element abundances [27–30] is in strong agreement with SM prediction [31–45]. This makes N_{eff} a powerful tool in testing BSM physics that affects early universe cosmology before recombination [22, 46–69]. We carry out the full Boltzmann evolution, allowing the X boson to “freeze in” [70], become nonrelativistic, redshift as matter, and then decay back into SM states, modifying ΔN_{eff} . Earlier calculations have considered the contributions to ΔN_{eff} from the freeze in of a dark photon [62] and $U(1)_{\mu-\tau}$ [22]. The cosmological constraints from ΔN_{eff} on the dark photon are relatively strong when the dark photon mass is near the temperature of BBN, ~ 1 MeV, when the dark photon can interact with the electron plasma and thus (indirectly) affect the neutrino energy density, but weaker below this since the dark photon does not interact with neutrinos. By contrast, mediators that freeze in from their interactions with neutrinos have substantially stronger constraints, e.g., $U(1)_{\mu-\tau}$ [22]. In this paper, we utilize the formalism and approximations outlined in [22, 60, 63], extended and applied to the case of a $U(1)_{B-L}$ gauge boson.

The central observation is that an out-of-equilibrium abundance of new particles that interact with the SM can be well approximated by using *equilibrium* distributions with nonzero chemical potentials. We will discuss the formalism and approximations in detail, as applied to $U(1)_{B-L}$. The result is that since $U(1)_{B-L}$ has a nonzero coupling to neutrinos, there are strong bounds from ΔN_{eff} from the CMB that get *stronger* with *decreasing* mass of X , down to of order $m_X \sim 1$ eV. In the regime $m_X < 2m_e$, our results are qualitatively consistent with a similar analysis done for $U(1)_{\mu-\tau}$ [22]. At even smaller masses, $m_X \lesssim 1$ eV, fifth force constraints [71–74] become very strong and dominate the bounds [12]. For gauge boson masses near (and below) 1 eV, a more sophisticated treatment of the CMB is necessary to fully elucidate cosmological bounds. We will comment on this in the Discussion.

To our knowledge, the first paper that considered constraints on the mass and coupling of a light $U(1)_{B-L}$ gauge boson from its effects on ΔN_{eff} is [75]. They considered a light $U(1)_{B-L}$ gauge boson with just left-handed neutrinos among the fermionic relativistic degrees of freedom. The critical difference between our study and [75] is that the latter only considered the constraints from ΔN_{eff} from BBN, using simple thermalization scaling arguments. Ref. [75] found that for $m_X \gtrsim 10$ MeV, requiring the scattering process $e^- \nu \rightarrow e^- \nu$ through

off-shell X exchange is not larger than the weak interaction sets a constraint. We verify this constraint also applies to ΔN_{eff} measured by the CMB, using our Boltzmann equation evolution. Ref. [75] also considered $m_X < 10$ MeV. In this region, [75] required only that $X \leftrightarrow \nu\bar{\nu}$ did not reach thermal equilibrium at $T \sim 1$ MeV, so that X does not contribute excessively to ΔN_{eff} during BBN. As we will see, we find much stronger constraints in the region $m_X < 10$ MeV from detailed numerical calculations of ΔN_{eff} at the CMB era as well as strong constraints on the helium mass fraction Y_p , at the BBN era.

There are also constraints on *very* weakly coupled mediators that are completely out-of-equilibrium, but decay on timescales that can disrupt BBN [76–78] or to cause spectral distortion in the CMB [54, 64, 79]. We show these constraints on the parameter space of $U(1)_{B-L}$, obtained from [64], that are complementary to our results.

2 Gauged $U(1)_{B-L}$: Majorana and Dirac neutrino cases

$U(1)_{B-L}$ is among the most interesting possible new forces since it is the only flavor-universal global symmetry of the SM that is gaugeable. All mixed $U(1)_{B-L} \times \text{SM}^2$ anomalies automatically vanish within the SM. The $[U(1)_{B-L}]^3$ anomaly remains, requiring additional chiral fermions that transform under just $U(1)_{B-L}$. The simplest solution is to add one chiral fermion per generation with lepton number equal and opposite to ν_L , namely, one right-handed neutrino per generation.

To establish notation, gauged $U(1)_{B-L}$ is mediated by a vector boson X^μ that interacts with the SM quarks and leptons with charge

$$q_f = (B - L)_f = \begin{cases} +1/3 & Q_L, u_R, d_R \\ -1 & L, e_R, \nu_R \end{cases}, \quad (2.1)$$

where we have written the fermions in four-component notation consistent with [80]. We assume $U(1)_{B-L}$ is broken, and so X acquires a mass m_X . The spontaneous breaking of $U(1)_{B-L}$ can be accomplished by introducing a complex scalar, ϕ_X , transforming under $B - L$ with charge q_X , and gauge coupling g_X , with a potential engineered to spontaneously break the symmetry. The scalar Lagrangian is

$$\mathcal{L} = (D_\mu \phi_X)^\dagger D^\mu \phi_X - V(\phi_X) \quad (2.2)$$

where $D^\mu \equiv \partial^\mu - ig_X q_X X^\mu$, with

$$V(\phi_X) = \lambda_X \left(\phi_X^\dagger \phi_X - \frac{v_X^2}{2} \right)^2 \quad (2.3)$$

and the minimum of the scalar potential occurs at $\langle \phi_X \rangle = v_X/\sqrt{2}$. Expanding around the minimum, with $\phi_X = (h_X + v_X)/\sqrt{2}$, where h_X is the $B - L$ Higgs boson, the physical states in the theory have masses

$$X^\mu : \quad m_X = g_X q_X v_X \quad (2.4)$$

$$h_X : \quad m_{h_X}^2 = 2\lambda_X v_X^2. \quad (2.5)$$

Throughout the paper, we work in the limit $g_X q_X \ll \lambda_X$, and so, $m_X \ll m_{h_X}$. Consequently, we will not need to consider the h_X participating in the degrees of freedom in the thermal bath for ΔN_{eff} calculations. The ability to adjust the $B - L$ charge of ϕ_X implies m_X can be made arbitrarily small relative to $g_X v_X$. That is, from the perspective of the gauge and Higgs sector, one can independently adjust m_X and g_X (as well as m_{h_X} , through λ_X).

2.1 Neutrino masses: Majorana and Dirac cases

We do need to address neutrino masses. Given that $U(1)_{B-L}$ is gauged, the usual dimension-5 Weinberg operator for Majorana neutrino masses, $(LH)^2/\Lambda$, is forbidden. Instead, Yukawa couplings of left-handed and right-handed neutrinos are permitted,

$$y_D^{ij} \bar{L}_i H^\dagger \nu_{R,j} + h.c., \quad (2.6)$$

giving neutrinos Dirac masses that preserve $U(1)_{B-L}$. This “**Dirac case**” is one of the two cases we will consider in this paper. In the Dirac case, since neutrinos acquire their mass from Yukawa couplings to the SM Higgs field, there is (still) no restriction on the ability to adjust m_X and g_X independently.

The alternative, “**Majorana case**”, is one where the right-handed neutrinos that are required to cancel the $[U(1)_{B-L}]^3$ anomaly acquire Majorana masses after $U(1)_{B-L}$ is spontaneously broken. When combined with the Dirac mass terms, equation (2.6), after electroweak symmetry is broken, this leads to the usual see-saw formula that results in left-handed neutrinos acquiring small Majorana masses. Right-handed neutrinos can acquire mass with just one Higgs field transforming under $U(1)_{B-L}$ if the $B-L$ charge is fixed to be $q_X = \pm 2$, such that Yukawa-like interactions are permitted,

$$\frac{y_M^{ij}}{2} \nu_{R,i}^c \nu_{R,j}^c \phi_X^{(\dagger)} + h.c., \quad (2.7)$$

where $\nu_{R,i}^c$ are the right-handed neutrinos written with 2-component left-handed fermion notation (in order to avoid Majorana notation). In this scenario, the vev of ϕ_X not only gives mass to the gauge boson, but it also gives Majorana masses to the right-handed neutrinos, $M_R \sim y_M v_X$.

For us, the key distinction is that in the Majorana case, the right-handed neutrinos can be much heavier, and thus not contribute in any way to ΔN_{eff} . This is in contrast to the Dirac scenario, where if the right-handed neutrinos were ever in equilibrium (through, for example, X^μ exchange), they necessarily contribute to ΔN_{eff} [61, 65, 81]. The size of the contribution to ΔN_{eff} is controlled just by the dilution of the number of relativistic degrees of freedom after heavier SM fields annihilate (or decay) and dump their entropy into the photon bath.

It is interesting to consider the bounds on the Majorana masses for right-handed neutrinos from cosmology. Obviously if the right-handed neutrinos were in thermal equilibrium with the SM, they would excessively contribute to ΔN_{eff} during BBN and CMB if their mass were less than approximately 10 MeV. Thermal equilibrium is naturally achieved through X^μ exchange, so long as g_X is not excessively small. (We’ll quantify this in detail later in the paper.) Once the right-handed neutrinos are heavier than about 10 MeV, their abundance would be at least somewhat suppressed as they become nonrelativistic once the temperature of the Universe drops well below their mass.

Even if right-handed neutrinos decoupled early in the Universe, they can and will decay to left-handed neutrinos and a (possibly off-shell) Higgs boson, with a significant suppression in the rate due to the smallness of the (Dirac) Yukawa coupling of the right-handed neutrinos to the left-handed neutrinos. In appendix A, we estimate the rate, and find that for $M_R \gtrsim 20$ GeV, the right-handed neutrinos decay before the onset of BBN.

Finally, it is also instructive to consider the case where $U(1)_{B-L}$ is explicitly broken without any scalar sector, i.e., a Stückelberg mass for the X vector field (for a recent detailed

discussion of the Stückelberg mechanism, see [82]). In the Dirac scenario, we can stop there, since Dirac masses respect $U(1)_{B-L}$ (see also [13]). (This is equivalent, in the spontaneously broken theory, to holding $m_X = q_X g_X v_X$ fixed, λ_X fixed, but then taking $q_X \ll 1$ while v_X is taken large. This limit permits any (perturbative) value for g_X .) In the Majorana case, we must also explicitly break $U(1)_{B-L}$ by 2 units when writing explicit Majorana masses $(M_R)_{ij} \nu_i^c \nu_j^c + h.c.$. The explicit breaking implies the $[U(1)_{B-L}]^3$ anomaly will appear below the scale M_R . Thus, the right-handed neutrinos induce a 3-loop anomalous contribution to the mass of the (Stückelberg) X^μ vector field. The size of this contribution is easily estimated [83, 84]

$$\Delta m_X \simeq \frac{g_X^3 M_R}{64\pi^3} \quad (2.8)$$

which implies a lower bound on the mass of X^μ that decreases rapidly as g_X is lowered. This bound is always weaker than equation (A.4), so that if we require right-handed neutrinos decay before BBN, there is no further constraint. Only if M_R were large, such as a traditional see-saw mechanism with $y_D \sim 1$, with $M_R \sim 10^{14-15}$ GeV, would there be any constraint at all on g_X , though even then this constraint is quite mild.

3 Effective number of relativistic species: N_{eff}

In standard cosmology at temperature $T \sim 10$ MeV [85], electrons, photons, and neutrinos were in thermal equilibrium. As the universe cooled, the weak interaction rate dropped below the Hubble expansion rate and neutrinos decoupled from the electromagnetic plasma around $T \sim 2$ MeV. As the universe continued to cool, the temperature dropped below the electron mass, e^+e^- annihilation depleted the vast majority of charged leptons. In the limit of instantaneous neutrino decoupling, the electron-positron entropy was transferred solely to photons resulting in a temperature ratio of $T_\gamma/T_\nu = (11/4)^{1/3} \approx 1.401$ after annihilation completed. However, the weak interaction remained slightly active during e^+e^- annihilation, resulting in a small but appreciable heating of neutrinos. This gives rise to a small increase to the energy density of neutrinos, conventionally defined by the *effective number of relativistic species*,

$$N_{\text{eff}} = \frac{8}{7} \left(\frac{11}{4} \right)^{4/3} \left(\frac{\rho_{\text{rad}} - \rho_\gamma}{\rho_\gamma} \right), \quad (3.1)$$

which is the ratio of non-photon to photon radiation density. Any new BSM radiation density present well before recombination can be treated as an additional contribution to N_{eff} . The normalization in equation (3.1) is chosen such that $N_{\text{eff}} = N_\nu = 3$ in the instantaneous neutrino decoupling limit.

The state-of-the-art calculation in the SM gives $N_{\text{eff}}^{\text{SM}} = 3.045\text{--}3.046$, that takes into higher order corrections, non-thermal neutrino distribution functions, neutrino oscillations, etc. [31, 32]. In this paper, we have followed Refs. [60, 63] that have provided an efficient calculation of N_{eff} which employs certain approximations that nevertheless result in excellent accuracy, which we will discuss in detail in section 4.1. For instance, using this method, we obtain the photon-to-neutrino temperature ratio, the neutrino chemical potential, and N_{eff} in the SM

$$T_\gamma/T_\nu = 1.3945, \quad \mu_\nu/T_\nu = -4.82 \times 10^{-3}, \quad N_{\text{eff}}^{\text{SM}} = 3.042. \quad (3.2)$$

The point of re-doing the SM calculation here is to demonstrate that we can achieve reasonable accuracy of N_{eff} even with the approximations that have been employed. The very small $\sim 0.1\%$ discrepancy between our calculation and the precise determination is slightly accidental – some of the effects we have neglected, that contribute at a level of $\sim 0.3\%$, happen to very nearly cancel out when summed together (see [63] for details). In any case, our calculation is able to reproduce the non-instantaneous decoupling of neutrinos in the SM to an accuracy of order $\Delta N_{\text{eff}} \sim 0.01$.

After e^+e^- annihilation is complete, the number of relativistic degrees of freedom remains the same in the SM down to the CMB era.¹ In the presence of physics beyond the SM, there can be new degrees of freedom that appear (or disappear) before or after BBN. This can be characterized by the number of relativistic degrees of freedom at CMB, $N_{\text{eff}}^{\text{CMB}}$, to be distinguished from the number of relativistic degrees of freedom at BBN, $N_{\text{eff}}^{\text{BBN}}$. In this paper, N_{eff} refers exclusively to $N_{\text{eff}}^{\text{CMB}}$, and hereafter N_{eff} and ΔN_{eff} refer to the quantities at the CMB era. We do, however, calculate the shift to the helium mass fraction Y_p at BBN, separately from ΔN_{eff} . We will present our calculations of N_{eff} in section 5 and Y_p in section 7, and compare to the observational determinations at the end of each of those sections.

4 Early universe thermodynamics

Our method to calculate thermodynamic quantities in the early universe utilizes several approximations in order to solve the Boltzmann equations that were described in detail in [60, 63].² The key insight from [60, 63] is that we can approximate the effects of out-of-equilibrium (“freeze-in”) X bosons using *equilibrium* distributions with nonzero chemical potentials. How this works requires some explanation. At temperatures near BBN, the dominant contributions to the energy density are from electrons (and positrons), photons, and neutrinos. In the SM, the annihilation and scattering rates between electrons, positrons, and photons is very efficient ensuring $T_\gamma = T_e$. Since photon number is not conserved, the processes $e^+e^- \leftrightarrow \gamma$, $e^+e^- \leftrightarrow \gamma\gamma$, and $e^+e^- \leftrightarrow \gamma\gamma\gamma$ imply that the chemical potential for photons, electrons and positrons vanishes, $\mu_\gamma = \mu_e = 0$ (to a very good approximation [86]). When neutrino-electron scattering is active for temperatures $T \gtrsim 2$ MeV, the processes $e^+e^- \leftrightarrow \bar{\nu}_\alpha\nu_\alpha$, $e^\pm\nu_\alpha \leftrightarrow e^\pm\nu_\alpha$, and $e^\pm\bar{\nu}_\alpha \leftrightarrow e^\pm\bar{\nu}_\alpha$ ensure that $\mu_\nu \simeq 0$. Hence, in the SM, chemical potentials do not play a critical role in determining the thermodynamic evolution near and below the BBN era.

When we introduce a light $U(1)_{B-L}$ gauge boson X , there are three possible regimes of interest: heavy ($m_X \gg 1$ MeV), intermediate ($m_X \sim 1$ MeV), and light ($m_X \ll 1$ MeV). In all regimes, we assume $\mu_\gamma = \mu_e = 0$ throughout the Boltzmann evolution, given that the electromagnetic interactions will always be much faster than interactions among X bosons. Nevertheless, we allow for chemical potentials for X and neutrinos to develop and evolve with temperature, as X freezes-in through its very weak interactions with the SM. As we will see, the thermodynamic evolution of the SM particles plus X will be quite different in these different regimes.

¹We do not need to consider SM neutrino masses, since they are bounded to be smaller than the temperatures we consider in the paper [26].

²We have benefited from viewing the code `NUDEC_BSM` as a reference to setup our calculations. However, all of our calculations are based on our own code.

In the heavy regime, $m_X \gg 1$ MeV, as the temperature drops below m_X , the X bosons become nonrelativistic while the weak interactions that keep electrons and neutrinos in thermal and chemical equilibrium remain active. At these high temperatures, there is competition between $1 \leftrightarrow 2$ processes involving $X \leftrightarrow \nu\bar{\nu}$, that will cause μ_X and μ_ν to develop, and the electroweak-mediated $2 \leftrightarrow 2$ processes, that drive $\mu_\nu \rightarrow 0$. Initially, X is out-of-equilibrium, and so a chemical potential for X and neutrinos can (and will) develop. As the temperatures decrease, X becomes nonrelativistic, the $2 \leftrightarrow 2$ processes dominate, driving μ_ν (and μ_X) to small values. At still larger masses, for temperatures $10 \text{ MeV} \lesssim T \ll m_X$, the $1 \leftrightarrow 2$ processes are irrelevant, and instead off-shell X -exchange can contribute to $2 \leftrightarrow 2$ processes qualitatively similar to electroweak gauge boson exchange. Here, there is a constraint on the strength of the X boson interactions with the SM that arises from delaying neutrino freeze-out, but this is much weaker than the constraints from lighter masses, as we will see below.

In the light regime, when $m_X \ll 1$ MeV, electron-positron annihilation is fully complete, leaving only photons, neutrinos, and X as the relativistic degrees of freedom. In this regime, neutrinos are out of thermal and chemical equilibrium with the SM, and thus as X freezes-in, the evolution of Boltzmann equations result in a chemical potential for X and neutrinos through the process is $X \leftrightarrow \nu\bar{\nu}$. If this is efficient enough to reach chemical equilibrium, $\mu_X = 2\mu_\nu$. Note that since $U(1)_{\text{B-L}}$ is flavor-conserving, we necessarily have $\mu_\nu = \mu_{\bar{\nu}}$.

Finally, the intermediate regime, $m_X \sim 1$ MeV, is the trickiest one to model. When $T \sim 1$ MeV, the weak interactions have recently decoupled, and so the $2 \leftrightarrow 2$ electroweak processes that enforce $\mu_\nu \simeq 0$ have just recently shut off. This means that as a chemical potential for μ_X develops from its out-of-equilibrium production, the resulting μ_ν that also develops, can remain. However, electron-photon interactions are in thermal and chemical equilibrium, and so $\mu_e = 0$. If X were to be in thermal equilibrium with both electrons and neutrinos, the electron interactions $X \leftrightarrow e^+e^-$ would bias $\mu_X \simeq 0$. Instead, when X is out-of-equilibrium, a chemical potential for X can develop as X freezes-in from both $e^+e^- \rightarrow X$ and $\nu\bar{\nu} \rightarrow X$ interactions. As the universe cools, more X is produced, but then e^+e^- annihilation into photons rapidly depletes the electron-positron bath. This means X could reach thermal equilibrium with neutrinos, with a nonzero chemical potential, since the remaining electrons and positrons have dropped out of chemical equilibrium.

4.1 Approximations

We assume that all fermions and bosons follow Fermi-Dirac (FD, positive) and Bose-Einstein (BE, negative), $f(E) = [e^{(E-\mu)/T} \pm 1]^{-1}$ distribution functions respectively. This assumption is well-established when the energy and momentum exchange between particles is efficient. If interactions are not fully efficient, i.e. out-of-equilibrium evolution, distributions may obtain spectral distortion corrections. An example of this is shown in figures 9,10 of [22] for the case of $U(1)_{L_\mu-L_\tau}$. These corrections are expected to be small.

We assume, to an excellent approximation, that the electron/positron plasma is highly thermalized with the photon plasma such that $T_\gamma = T_e$ and $\mu_\gamma = \mu_e = 0$. Here, we leverage the strong annihilation and scattering rate between electrons, positrons, and photons and that the number of photons is not conserved in the early universe. As for neutrinos, we describe a neutrino fluid with a single distribution characterized by $T_\nu \equiv T_{\nu_e} = T_{\nu_\mu} = T_{\nu_\tau}$ and μ_ν . Here, we ignored neutrino oscillations which become active for temperatures $T = 3\text{--}5$ MeV, [87, 88], and model this effect by setting the temperature of the different neutrino species equal. The correction due to neutrino oscillations in SM is $\Delta N_{\text{eff}} = 0.0007$ [31]. The

correction due to evolving distinct neutrino species temperature rather than a single T_ν was found to be $\Delta N_{\text{eff}} = 0.001$ using the approximations [60, 63] we employ in this paper.

For the collision terms we have implemented the correct particle distributions for the $1 \leftrightarrow 2$ collision terms, and approximate particle distributions for $2 \leftrightarrow 2$ collision terms. For the $1 \leftrightarrow 2$ processes, this means we use a Fermi-Dirac distribution for fermions, a Bose-Einstein distribution for bosons, and include Pauli blocking and Bose enhancement. For the $2 \leftrightarrow 2$ processes, we use Maxwell-Boltzmann distributions for all particles, which reduces the number of integrations needed for the collision terms and significantly decreases the numerical computation time. Our implementation of using the correct statistics for the $1 \leftrightarrow 2$ collision processes is motivated by the relative importance of these processes in determining an accurate calculation of N_{eff} . While the qualitative features of our results remain unaffected even if Maxwell-Boltzmann distributions were used for $1 \leftrightarrow 2$ processes, quantitatively we find that the contours of ΔN_{eff} shift to slightly overestimate the impact of the X boson within the (m_X, g_X) parameter space.

Finally, we have also taken into account finite temperature effects that result from shifts in the masses and self-energies from their vacuum values. In the SM, these finite temperature effects [39, 60, 89] result in an $\mathcal{O}(0.01)$ correction to N_{eff} . We have outlined the relevant finite temperature effects in appendix B, where we show that for the case $m_X > 2m_e$, these corrections yield at most 1 – 2% shift relative to the vacuum evolution, and so we neglect them in this regime. This result is consistent with [90] where finite temperature corrections to the dark photon in early universe were found to be negligible in this mass range. However, for $m_X < 2m_e$, finite temperature corrections become important when the e^+e^- interactions contribute significantly to the X abundance, as discussed in section 4.3.3.

4.2 Boltzmann equations

The distribution for a particle species f evolves in accordance with the Liouville equation

$$\frac{\partial f}{\partial t} - H p \frac{\partial f}{\partial p} = \mathcal{C}[f], \quad (4.1)$$

for particle momentum p , Hubble expansion rate $H = \sqrt{8\pi\rho_{\text{tot}}/(3M_{\text{Pl}}^2)}$, and distribution dependent collision term $\mathcal{C}[f]$. The collision terms account for interactions affecting particle distributions, i.e., decays, annihilations, scattering, and their inverse processes.

With the approximations discussed in section 4.1, the Liouville equation in equation (4.1) can be reformulated in terms of the distribution's temperature and chemical potential,

$$\frac{dT_i}{dt} = \mathbb{D}(T_i, \mu_i) \left[-3H \left((\rho_i + P_i) \frac{\partial n_i}{\partial \mu_i} - n_i \frac{\partial \rho_i}{\partial \mu_i} \right) + \frac{\partial n_i}{\partial \mu_i} \frac{\delta \rho_i}{\delta t} - \frac{\partial \rho_i}{\partial \mu_i} \frac{\delta n_i}{\delta t} \right], \quad (4.2a)$$

$$\frac{d\mu_i}{dt} = -\mathbb{D}(T_i, \mu_i) \left[-3H \left((\rho_i + P_i) \frac{\partial n_i}{\partial T_i} - n_i \frac{\partial \rho_i}{\partial T_i} \right) + \frac{\partial n_i}{\partial T_i} \frac{\delta \rho_i}{\delta t} - \frac{\partial \rho_i}{\partial T_i} \frac{\delta n_i}{\delta t} \right], \quad (4.2b)$$

$$\mathbb{D}(T, \mu) = \left(\frac{\partial n}{\partial \mu} \frac{\partial \rho}{\partial T} - \frac{\partial n}{\partial T} \frac{\partial \rho}{\partial \mu} \right)^{-1}. \quad (4.2c)$$

Here n, ρ, P are the number, energy, and pressure densities for a particle i with d_i degrees of freedom obtained by integrating f over $d_i d^3p/(2\pi)^3$, $d_i E d^3p/(2\pi)^3$, and $d_i \frac{p^2}{3E} d^3p/(2\pi)^3$ respectively. $\delta n/\delta t$ and $\delta \rho/\delta t$ are the number and energy transfer rates between particle

species obtained by integrating $\mathcal{C}[f]$ over the same measures. The formulae for these thermodynamic quantities and their derivatives can be found in appendix A.6 of [63]. Explicitly, the seven Boltzmann equations parameterizing our system are given by

$$\begin{aligned}
\frac{dT_X}{dt} &= \mathbb{D}(T_X, \mu_X) \left[-3H \left((\rho_X + P_X) \frac{\partial n_X}{\partial \mu_X} - n_X \frac{\partial \rho_X}{\partial \mu_X} \right) + \frac{\partial n_X}{\partial \mu_X} \frac{\delta \rho_X}{\delta t} - \frac{\partial \rho_X}{\partial \mu_X} \frac{\delta n_X}{\delta t} \right], \\
\frac{dT_{\nu_R}}{dt} &= \mathbb{D}(T_{\nu_R}, \mu_{\nu_R}) \left[-3H \left((\rho_{\nu_R} + P_{\nu_R}) \frac{\partial n_{\nu_R}}{\partial \mu_{\nu_R}} - n_{\nu_R} \frac{\partial \rho_{\nu_R}}{\partial \mu_{\nu_R}} \right) + \frac{\partial n_{\nu_R}}{\partial \mu_{\nu_R}} \frac{\delta \rho_{\nu_R}}{\delta t} - \frac{\partial \rho_{\nu_R}}{\partial \mu_{\nu_R}} \frac{\delta n_{\nu_R}}{\delta t} \right], \\
\frac{dT_{\nu_L}}{dt} &= \mathbb{D}(T_{\nu_L}, \mu_{\nu_L}) \left[-3H \left((\rho_{\nu_L} + P_{\nu_L}) \frac{\partial n_{\nu_L}}{\partial \mu_{\nu_L}} - n_{\nu_L} \frac{\partial \rho_{\nu_L}}{\partial \mu_{\nu_L}} \right) + \frac{\partial n_{\nu_L}}{\partial \mu_{\nu_L}} \frac{\delta \rho_{\nu_L}}{\delta t} - \frac{\partial \rho_{\nu_L}}{\partial \mu_{\nu_L}} \frac{\delta n_{\nu_L}}{\delta t} \right], \\
\frac{dT_\gamma}{dt} &= \left(\frac{\partial \rho_\gamma}{\partial T_\gamma} + \frac{\partial \rho_e}{\partial T_\gamma} \right)^{-1} \left[4H \rho_\gamma + 3H(\rho_e + P_e) + \frac{\delta \rho_e}{\delta t} \right], \\
\frac{d\mu_X}{dt} &= -\mathbb{D}(T_X, \mu_X) \left[-3H \left((\rho_X + P_X) \frac{\partial n_X}{\partial T_X} - n_X \frac{\partial \rho_X}{\partial T_X} \right) + \frac{\partial n_X}{\partial T_X} \frac{\delta \rho_X}{\delta t} - \frac{\partial \rho_X}{\partial T_X} \frac{\delta n_X}{\delta t} \right], \\
\frac{d\mu_{\nu_R}}{dt} &= -\mathbb{D}(T_{\nu_R}, \mu_{\nu_R}) \left[-3H \left((\rho_{\nu_R} + P_{\nu_R}) \frac{\partial n_{\nu_R}}{\partial T_{\nu_R}} - n_{\nu_R} \frac{\partial \rho_{\nu_R}}{\partial T_{\nu_R}} \right) + \frac{\partial n_{\nu_R}}{\partial T_{\nu_R}} \frac{\delta \rho_{\nu_R}}{\delta t} - \frac{\partial \rho_{\nu_R}}{\partial T_{\nu_R}} \frac{\delta n_{\nu_R}}{\delta t} \right], \\
\frac{d\mu_{\nu_L}}{dt} &= -\mathbb{D}(T_{\nu_L}, \mu_{\nu_L}) \left[-3H \left((\rho_{\nu_L} + P_{\nu_L}) \frac{\partial n_{\nu_L}}{\partial T_{\nu_L}} - n_{\nu_L} \frac{\partial \rho_{\nu_L}}{\partial T_{\nu_L}} \right) + \frac{\partial n_{\nu_L}}{\partial T_{\nu_L}} \frac{\delta \rho_{\nu_L}}{\delta t} - \frac{\partial \rho_{\nu_L}}{\partial T_{\nu_L}} \frac{\delta n_{\nu_L}}{\delta t} \right].
\end{aligned} \tag{4.3}$$

The ν_R equations are included only in the Dirac case. The transfer rates $\delta n_i/\delta t$ and $\delta \rho_i/\delta t$ will be discussed in the next section.

4.3 Collision terms

4.3.1 Electron-neutrino interactions

In the SM, the relevant interactions between electrons and left-handed neutrinos are the weak interactions $e^+e^- \leftrightarrow \bar{\nu}_\alpha \nu_\alpha$, $e^\pm \nu_\alpha \leftrightarrow e^\pm \nu_\alpha$, and $e^\pm \bar{\nu}_\alpha \leftrightarrow e^\pm \bar{\nu}_\alpha$. The transfer rates for these processes are given by [63]

$$\frac{\delta \rho_{e-\nu}^{\text{SM}}}{\delta t} = 2 \frac{G_F^2}{3\pi^5} \left[C_V^2 + C_A^2 + 2 \left(\tilde{C}_V^2 + \tilde{C}_A^2 \right) \right] F_\rho(T_\gamma, T_\nu, \mu_\nu) \tag{4.4a}$$

$$\frac{\delta n_{e-\nu}^{\text{SM}}}{\delta t} = 16 \frac{G_F^2}{3\pi^5} \left[C_V^2 + C_A^2 + 2 \left(\tilde{C}_V^2 + \tilde{C}_A^2 \right) \right] F_n(T_\gamma, T_\nu, \mu_\nu). \tag{4.4b}$$

Here we defined

$$F_\rho(T_\gamma, T_\nu, \mu_\nu) = 32 (T_\gamma^9 - T_\nu^9 e^{\frac{2\mu_\nu}{T_\nu}}) + 56 T_\gamma^4 T_\nu^4 e^{\frac{\mu_\nu}{T_\nu}} (T_\gamma - T_\nu), \tag{4.5a}$$

$$F_n(T_\gamma, T_\nu, \mu_\nu) = T_\gamma^8 - T_\nu^8 e^{\frac{2\mu_\nu}{T_\nu}}. \tag{4.5b}$$

with $C_V = g_L^{\nu e} + g_R^{\nu e} = \frac{1}{2} + 2s_W^2$, $C_A = g_L^{\nu e} - g_R^{\nu e} = \frac{1}{2}$, $\tilde{C}_V = g_L^{\nu\mu,\tau} + g_R^{\nu\mu,\tau} = -\frac{1}{2} + 2s_W^2$, and $\tilde{C}_A = g_L^{\nu\mu,\tau} - g_R^{\nu\mu,\tau} = -\frac{1}{2}$ being the weak vector and axial couplings, $s_W^2 \simeq 0.223$ is the weak mixing angle, and $G_F \simeq 1.16 \times 10^{-11} \text{ MeV}^{-2}$ is the Fermi constant.

These interactions mediated by weak boson exchange can also be mediated by X -exchange. Since the weak interactions drop out-of-equilibrium near $T \sim 1 \text{ MeV}$, we are interested in the strength of X -exchange interactions when X can also be integrated out. For $m_X \gtrsim 10 \text{ MeV}$, we can write the effective interaction Lagrangian

$$\mathcal{L}_{\text{int}} = -\frac{g_X^2}{m_X^2} [(\bar{\nu}_L \gamma^\alpha \nu_L + \bar{\nu}_R \gamma^\alpha \nu_R)] (\bar{e} \gamma_\alpha e). \tag{4.6}$$

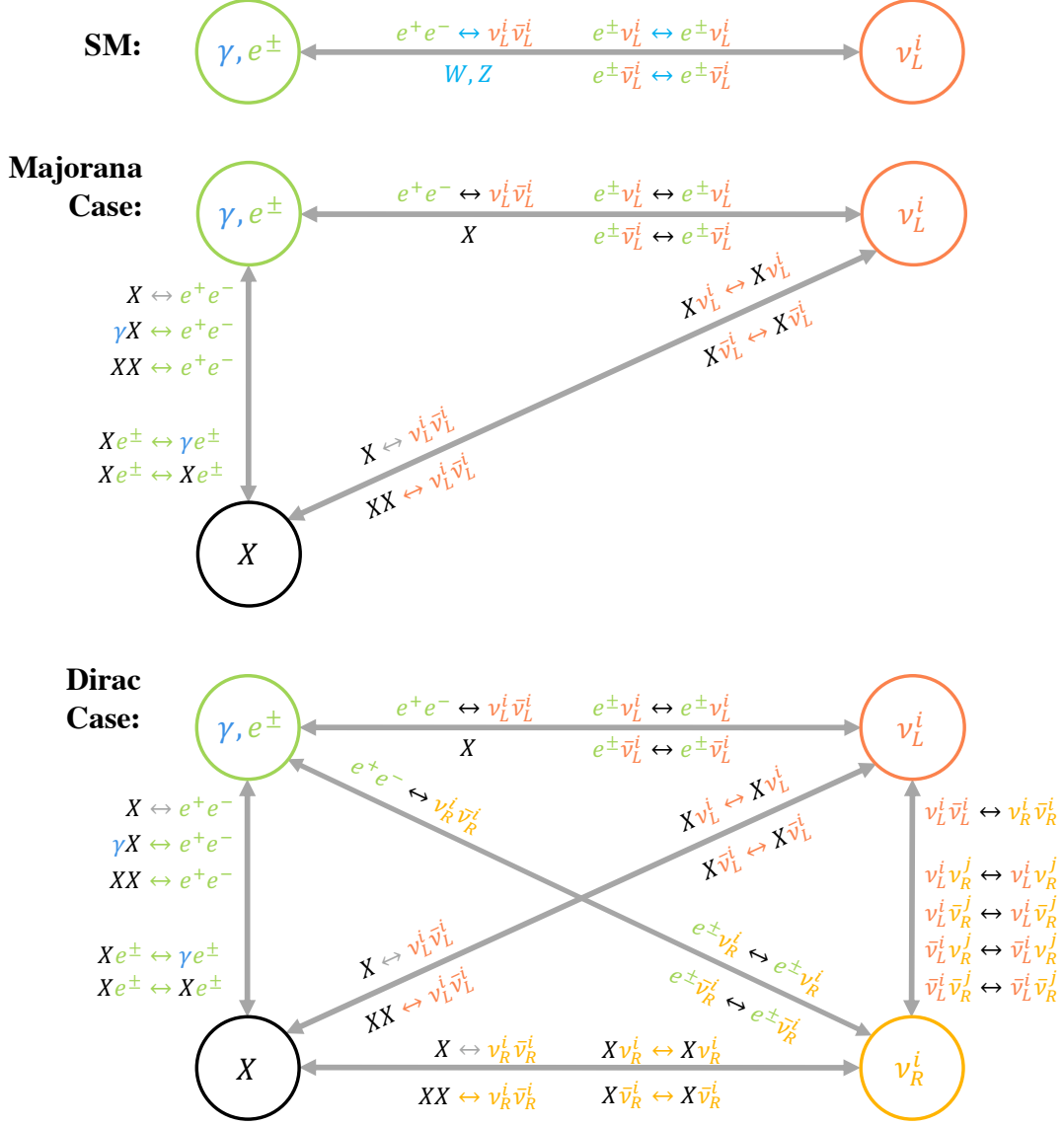


Figure 1. Summary of the processes considered in deriving the collision terms that relate different thermodynamic sectors in our model. All of the $1 \leftrightarrow 2$ processes are renormalizable contact interactions, while the $2 \leftrightarrow 2$ processes include all s, t , and u -channel exchange diagrams that preserve lepton number, electric charge, and flavor. Arrow color implies the mediator (or absence thereof): X (black); W, Z (light blue); ν_L^i (red); ν_R^i (yellow); and $1 \leftrightarrow 2$ contact interaction (grey).

The transfer rates now have the same form as equation (4.4) that only differs by the overall coefficient. Given that \tilde{C}_V and \tilde{C}_A correspond to the coefficients for just Z -exchange in the SM, we can obtain the transfer rate for X -exchange by setting $C_V = C_A = 0$ and $2(\tilde{C}_V^2 + \tilde{C}_A^2) \rightarrow 3q_X^2$, where X -exchange proceeds through a purely vector interaction with

charge $q_X^2 = 1$ for each lepton flavor, and $G_F \rightarrow \frac{g_X^2}{2\sqrt{2}m_X^2}$. The full $e - \nu$ transfer rates are

$$\frac{\delta\rho_{e-\nu}}{\delta t} = \frac{1}{3\pi^5} \left[G_F^2 (3 - 4s_W^2 + 24s_W^4) + \frac{3}{4} \frac{g_X^4}{m_X^4} \right] F_\rho(T_\gamma, T_\nu, \mu_\nu) \quad (4.7a)$$

$$\frac{\delta n_{e-\nu}}{\delta t} = \frac{8}{3\pi^5} \left[G_F^2 (3 - 4s_W^2 + 24s_W^4) + \frac{3}{4} \frac{g_X^4}{m_X^4} \right] F_n(T_\gamma, T_\nu, \mu_\nu). \quad (4.7b)$$

The X -exchange interaction can overpower the SM weak process when $g_X^2/m_X^2 \sim \mathcal{O}(G_F) \sim 10^{-11} \text{ MeV}^{-2}$. In this case, electron-neutrino (proton-neutron) decoupling is delayed to temperatures lower than that predicted in standard cosmology. As an extreme example, if the neutrino decoupling temperature was pushed below the electron-positron annihilation regime, then $T_\nu = T_\gamma$ today [as opposed to $T_\nu \sim (4/11)^{1/3} T_\gamma$], which would result in $N_{\text{eff}} \simeq 3(11/4)^{4/3} \simeq 11.6$

4.3.2 Decays and inverse decays

When kinematically accessible, the dominant BSM processes are $X \leftrightarrow e^+e^-$, $X \leftrightarrow \nu_L \bar{\nu}_L$, and $X \leftrightarrow \nu_R \bar{\nu}_R$. The partial decay widths of X to electron-positron or neutrino pair (left- or right-handed, one generation) is given by

$$\Gamma_{X \rightarrow e^+e^-} = \frac{g_X^2}{12\pi} m_X \left(1 + 2 \frac{m_e^2}{m_X^2} \right) \sqrt{1 - 4 \frac{m_e^2}{m_X^2}} \quad \Gamma_{X \rightarrow \nu_i \bar{\nu}_i} = \frac{g_X^2}{24\pi} m_X. \quad (4.8)$$

In Eq. 4.8, we use the vacuum value for the electron mass since we have verified that the finite temperature corrections shift our results only by a very small (at most 1-2%) amount (see Sec. 4.1 for details on our approximations). The collision term for the decay and inverse decay $X \leftrightarrow a\bar{a}$ is

$$\mathcal{C}_{X \rightarrow a\bar{a}}(p_X) = -\Gamma_{X \rightarrow a\bar{a}} \frac{m_X}{m_*} \frac{m_X}{E_X p_X} \int_{E_-}^{E_+} dE_a [f_X(1-f_a)(1-f_a) - f_a f_a(1+f_X)] \quad (4.9)$$

with $E_\pm^2 = p_X^2 + m_X^2$, $m_*^2 = m_X^2 - 4m_a^2$ and the bounds $E_\pm = \frac{1}{2}[E_X \pm (p_X m_*)/m_X]$. For example in $X \leftrightarrow \nu\bar{\nu}$, the first term in equation (4.9) is explicitly

$$f_X(1-f_a)(1-f_a) \longrightarrow f_X(E_X, T_X, \mu_X) [1 - f_\nu(E_\nu, T_\nu, \mu_\nu)] [1 - f_\nu(E_X - E_\nu, T_\nu, \mu_\nu)]. \quad (4.10)$$

The integral in equation (4.9), can be solved analytically taking a Bose-Einstein distribution for X and a Fermi-Dirac distribution for neutrinos and electrons, giving

$$\mathcal{C}_{X \rightarrow a\bar{a}} = -\Gamma_X \frac{m_X}{m_*} \frac{m_X T_a}{E_X p_X} \frac{e^{\frac{E_X}{T_a} + \frac{\mu_X}{T_X}} - e^{\frac{E_X}{T_X} + \frac{2\mu_a}{T_a}}}{\left(e^{\frac{E_X}{T_a}} - e^{\frac{2\mu_a}{T_a}} \right) \left(e^{\frac{E_X}{T_X}} - e^{\frac{\mu_X}{T_X}} \right)} \log \left[\frac{\left(e^{\frac{E_X}{T_a}} + e^{\frac{E_- + \mu_a}{T_a}} \right) \left(e^{\frac{E_+}{T_a}} + e^{\frac{\mu_a}{T_a}} \right)}{\left(e^{\frac{E_X}{T_a}} + e^{\frac{E_+ + \mu_a}{T_a}} \right) \left(e^{\frac{E_-}{T_a}} + e^{\frac{\mu_a}{T_a}} \right)} \right]. \quad (4.11)$$

Finally, the decay and inverse decay transfer terms are

$$\frac{\delta\rho_{X \leftrightarrow a\bar{a}}}{\delta t} = \frac{d_X}{(2\pi)^3} \int d^3 p_X E_X \mathcal{C}_{X \rightarrow a\bar{a}}(p_X) \quad (4.12a)$$

$$\frac{\delta n_{X \leftrightarrow a\bar{a}}}{\delta t} = \frac{d_X}{(2\pi)^3} \int d^3 p_X \mathcal{C}_{X \rightarrow a\bar{a}}(p_X) \quad (4.12b)$$

where $d_X = 3$ is the number of spin degrees of freedom of X .

4.3.3 Electron-X interactions

When $m_X < 2m_e$, the $X \leftrightarrow e^+e^-$ process is kinematically forbidden, and so the available e - X interactions are $\gamma X \leftrightarrow e^+e^-$ and $e^\pm X \leftrightarrow e^\pm \gamma$. These transfer rates can be derived following appendix A.7 of [63] giving,

$$\frac{\delta \rho_{2 \leftrightarrow 2}}{\delta t} = -\frac{d_1 d_2}{64\pi^4} \int_{s_{\min}}^{\infty} ds s \sigma_{2 \leftrightarrow 2}(s) \left[s T_\gamma K_2 \left(\frac{\sqrt{s}}{T_\gamma} \right) - \mathcal{A}(s, T_\gamma, T_X, \mu_X) \right], \quad (4.13a)$$

$$\frac{\delta n_{2 \leftrightarrow 2}}{\delta t} = -\frac{d_1 d_2}{64\pi^4} \int_{s_{\min}}^{\infty} ds s \sigma_{2 \leftrightarrow 2}(s) \left[2\sqrt{s} T_\gamma K_1 \left(\frac{\sqrt{s}}{T_\gamma} \right) - \mathcal{B}(s, T_\gamma, T_X, \mu_X) \right], \quad (4.13b)$$

where d_1, d_2 are the number of spin degrees of freedom of incoming particles 1 and 2, and $\sigma_{2 \leftrightarrow 2}$ is the cross section of the aforementioned interactions given in appendix C of [90], and

$$\mathcal{A}(s) = e^{\frac{\mu_X}{T_X}} \int dE_+ dE_- \frac{E_+ + E_-}{2} \exp \left[-\frac{E_+ - E_-}{2T_\gamma} \right] \exp \left[-\frac{E_+ + E_-}{2T_X} \right] \quad (4.14a)$$

$$\mathcal{B}(s) = e^{\frac{\mu_X}{T_X}} \int dE_+ dE_- \exp \left[-\frac{E_+ - E_-}{2T_\gamma} \right] \exp \left[-\frac{E_+ + E_-}{2T_X} \right] \quad (4.14b)$$

with $|E_- - E_+(m_2^2 - m_1^2)/s| \leq 2p_{12} \sqrt{(E_+^2 - s)/s}$, $p_{12} = [s - (m_1 + m_2)^2]^{1/2} [s - (m_1 - m_2)^2]^{1/2} / (2\sqrt{s})$, and $E_+ \geq \sqrt{s}$. Part of Eqs. (4.13), (4.14) can be evaluated analytically, while the remainder must be done numerically. To further simplify our evaluation of the phase space integrals in equation (4.14), we have taken $m_X = 0$, thereby slightly overestimating the integration region. In practice, this overestimate is only possibly relevant when $m_X \sim 2m_e$, and in this region, the $2 \rightarrow 2$ processes do not set the strongest bounds.

Finite temperature effects make significant corrections to these interactions, as we have explained in detail using analytic arguments presented in appendix B. In our Boltzmann evolution, we include these effects by replacing the vacuum coupling g_X in $\sigma_{2 \leftrightarrow 2}$ by the in-medium coupling

$$g_X^2 \longrightarrow g_{X,m}^2 = \frac{g_X^2 m_X^4}{[m_X^2 - m_\gamma(T)^2]^2 + [\text{Im } \Pi(T)]^2}, \quad (4.15)$$

where m_γ is the in-medium effective photon mass and $\text{Im } \Pi$ is the imaginary part of the photon polarization tensor. This demonstrates that there will be a *resonant enhancement* that occurs when $m_X = m_\gamma(T)$ at a specific temperature T_r for a given m_X . The in medium photon mass $m_\gamma(T)$ is calculated using the formalism in [91] for the real part of the photon polarization tensor. It should be noted that $m_\gamma(T)$ is also dependent on the photon energy, however, this weak dependence does not alter any dynamics and can be neglected. Our numerical evaluation of $m_\gamma(T)$ matches Eq. B.1 in the limits shown, $T \gg m_e$ and $T \ll m_e$. Next, we take $\text{Im } \Pi(T) = -\omega\Gamma$ as in Eq. B.7 [92]. We consider only Compton scattering and so $\Gamma = 8\pi\alpha^2/(3m_e^2)n_e$ (for $T \ll m_e$), $\Gamma \sim \alpha^2 T^2/(\pi\omega) \log(4T\omega/m_e^2)$ (for $T \gg m_e$) [90], and then take a linear interpolation between these two limiting expressions. Note that the kink in the $\Delta N_{\text{eff}} = 0.4, 0.5$ contours in figure 5 and $\Delta N_{\text{eff}} = 0.2$ and larger contours in figure 6 around $m_X \sim 50$ keV are a result of this linear interpolation. The contours on either side of the kink are accurate.

4.3.4 Suppressed interactions

In Table 1, we have shown several other interactions between X and the SM as well as interactions mediated by (virtual) X -exchange. We now briefly summarize the suppressions that these interactions have, and why we can neglect them in our evaluation of the Boltzmann evolution.

The interaction $e^+e^- \leftrightarrow XX$ is suppressed by a factor of g_X^2/e^2 compared to $e^+e^- \leftrightarrow \gamma X$. For the neutrino-mediated processes $\nu_L \bar{\nu}_L \leftrightarrow XX$ and $\nu_R \bar{\nu}_R \leftrightarrow XX$, the interaction rate $n_\nu \langle \sigma v \rangle_{\nu_i \bar{\nu}_i \leftrightarrow XX}$ is suppressed by an additional power of g_X^2 as compared to equivalent decay channels $X \leftrightarrow \nu_i \bar{\nu}_i$. Similarly, $Xe^\pm \leftrightarrow Xe^\pm$, $X\nu_L \leftrightarrow X\nu_L$, $X\nu_R \leftrightarrow X\nu_R$ are also suppressed by g_X^2 compared to the (inverse) decay processes, but in addition, also do not contribute to the change in number density of individual particle species. These interactions can be safely neglected.

In the Dirac neutrino case, there are additional processes involving right-handed neutrinos that arise, similar to the ones discussed in section 4.3.1. These include $e^+e^- \leftrightarrow \bar{\nu}_R \nu_R$, $e^\pm \nu_R \leftrightarrow e^\pm \nu_R$, $e^\pm \bar{\nu}_R \leftrightarrow e^\pm \bar{\nu}_R$ in the e - ν_R system and $\nu_L \bar{\nu}_L \leftrightarrow \nu_R \bar{\nu}_R$, $\nu_L \bar{\nu}_R \leftrightarrow \nu_L \bar{\nu}_R$, and $\nu_L \nu_R \leftrightarrow \nu_L \nu_R$ in the ν_L - ν_R system. We did not include X -exchange to right-handed neutrinos for the same reasons as above, namely, they are further suppressed by an additional power of g_X^2 .

4.4 Summary of transfer rates

Following the discussion of the collision terms, section 4.3, we now explicitly provide the transfer rates $\delta\rho_i/\delta t$ that we use in equation (4.3):

$$\frac{\delta\rho_X}{\delta t} = \frac{\delta\rho_{X\leftrightarrow e^+e^-}}{\delta t} + \frac{\delta\rho_{2\leftrightarrow 2}}{\delta t} + N_\nu \left[\frac{\delta\rho_{X\leftrightarrow \nu_L \bar{\nu}_L}}{\delta t} + \left\{ \frac{\delta\rho_{X\leftrightarrow \nu_R \bar{\nu}_R}}{\delta t} \right\} \right], \quad (4.16a)$$

$$\frac{\delta\rho_{\nu_R}}{\delta t} = \left\{ -\frac{1}{2} \frac{\delta\rho_{X\leftrightarrow \nu_R \bar{\nu}_R}}{\delta t} \right\}, \quad (4.16b)$$

$$\frac{\delta\rho_{\nu_L}}{\delta t} = \frac{1}{2} \left[\frac{\delta\rho_{e-\nu}}{\delta t} - \frac{\delta\rho_{X\leftrightarrow \nu_L \bar{\nu}_L}}{\delta t} \right], \quad (4.16c)$$

$$\frac{\delta\rho_\gamma}{\delta t} = -N_\nu \frac{\delta\rho_{e-\nu}}{\delta t} - \frac{\delta\rho_{X\leftrightarrow e^+e^-}}{\delta t} - \frac{\delta\rho_{2\leftrightarrow 2}}{\delta t}. \quad (4.16d)$$

Note that the neutrino Boltzmann equations in equation (4.3) evolve a single neutrino species (rather neutrino and anti-neutrino) which accounts for the factor of 1/2 in Eqs. (4.16b)-(4.16c). The $\delta n_i/\delta t$ rates can be straightforwardly deduced from Eqs. (4.16).

5 Numerical evolution of the Boltzmann equations and N_{eff}

We now discuss the details of solving the Boltzmann equations in equation (4.3) in order to determine the thermodynamic evolution of the universe with X interactions. The final result from this section, calculating the contours of ΔN_{eff} in the (m_X, g_X) parameter space, is the central result of this paper.

5.1 Initial conditions

We start with the initial condition $T_0 \equiv T_\gamma = T_{\nu_L} = \text{Max}[10 \text{ MeV}, 10 m_X]$. and $\mu_{\nu_L} = -10^{-5} T_0$. This ensures that all the dynamics before neutrino decoupling are captured. Furthermore, we start $T_X = T_{\nu_R} = 10^{-2} T_0$ and $\mu_X = \mu_{\nu_R} = -10^{-5} T_0$, so that both X and ν_R

begin with a negligible abundance compared to the SM bath, $\rho_X/\rho_\nu \sim 10^{-8}$. The specific (small) initial values of T_X, μ_X and their relation to T_{ν_R}, μ_{ν_R} do not impact the evolution, since the Boltzmann equations quickly evolve these quantities to their correct values.

The evolution of particle distributions is often shown as ρ_i/T_γ^4 , using T_γ to show dimensionless ratios of energy densities of different species. This is useful because in evolving over several orders of magnitude in temperature, a relativistic species energy density spans *many* orders of magnitude. Moreover, in cases where new physics does not affect photons, e.g. [22, 63], the evolution of T_γ can be used to provide a convenient measure of time that is independent of the new physics dynamics.

In our case, X interactions affect the evolution of photons, electrons, and neutrinos distributions. This means that in trying to compare the energy densities and number densities of different species with different choices of parameters (m_X, g_X), there can be differential effects on the evolution of T_γ , and thus both the numerator ρ_i and the denominator T_γ^4 . We therefore introduce a ‘‘reference’’ temperature, T_ξ , obtained by solving the Boltzmann equation $dT_\xi/dt = -HT_\xi$ with $T_\xi(t_0) = T_0$.³ In the following, we show energy and number densities scaled by T_ξ^4 or T_ξ^3 respectively, and this allows us to much more easily compare different choices of (m_X, g_X) with each other.

5.2 Evolution of Boltzmann equations

In this section, we discuss the solution to the Boltzmann equations in equation (4.3) at representative points in the parameter space. To do so, we examine the evolution of density and effective interaction rate for the particles in our system. The effective interaction rate⁴ is defined as

$$\frac{\langle \Gamma_i \rangle}{H} \equiv \frac{1}{HT_\xi^3} \frac{\delta n_i}{\delta t} \quad (5.1)$$

where $\delta n_i/\delta t$ is the sum of all number density transfer rates (section 4.4) for interactions between two species $i = X \leftrightarrow e$ or $X \leftrightarrow \nu$. This is the rate to which the forward or backward interaction dominate the other as compared to Hubble expansion rate. For example, a positive $\langle \Gamma_{X \leftrightarrow \nu} \rangle/H$ means the $\nu_i \bar{\nu}_i \rightarrow X$ dominates the backward rate and the neutrinos number density is decreasing in favor of X . Similarly, zero means forward/backward rates are equal and a zero plateau implies that X and neutrinos are thermalized while X is relativistic.

We first consider an example of an X boson that is light, $m_X = 10$ keV, that is representative of the light regime $m_X \ll 2m_e$. This is among the simpler cases since the $X \leftrightarrow e^+e^-$ process is kinematically forbidden and for sufficiently low coupling the only relevant interaction is $X \leftrightarrow \nu_L \bar{\nu}_L$. In figure 2, we show the scaled density and effective interaction rates for several values of $g_X = 10^{-10}$ to 10^{-12} . At the smaller end of the couplings, $g_X = 10^{-11}$ and $g_X = 10^{-12}$, neutrinos populate X without fully thermalizing (at $g_X = 10^{-11}$, $X \leftrightarrow \nu_L \bar{\nu}_L$ is almost thermalized). X then proceeds to evolve as matter $\rho_X \propto a^{-3}$ before dumping its entropy back into neutrinos. The nonrelativistic X 's decay into neutrinos that are now more

³One way to think about this is to imagine ξ is a (fictitious) massless particle with a temperature that is initially set to the temperature of the SM but is actually decoupled from all other particles. Taking ξ to be massless with an infinitesimal small number of degrees of freedom means ξ always evolves as radiation and does not affect Hubble expansion rate ($\rho_\xi \sim 0$).

⁴In [63], this quantity is instead defined as $(\delta n_{X \rightarrow \nu_i \bar{\nu}_i} \delta t)/(H n_\nu)$ for the one-way interaction. This is done to estimate the interaction strength at which X thermalizes with neutrinos, $\langle \Gamma_i \rangle \sim H$, without solving the Boltzmann equations. We replace n_ν by T_ξ^3 as we are also interested in electron interactions and $n_e \rightarrow 0$ after electron-positron annihilation. Secondly, we consider the forward and backward interaction in the transfer rates instead of just the forward rate [first term in square bracket of equation (4.12b)].

energetic than the primordial neutrino plasma that evolves as radiation $\rho_\nu \propto a^{-4}$. Therefore, the resulting neutrino energy density is larger than it would have been in the SM. This implies a positive N_{eff} is generated, as shown in the figure caption.

Also, in figure 2, for $g_X = 10^{-10}$, the most obvious feature is the resonance near $T_\xi \sim 0.15$ MeV resulting from the finite temperature corrections to $\gamma X \leftrightarrow e^+e^-$ and $e^\pm X \leftrightarrow e^\pm \gamma$. In fact, the resonance is also present at the same temperature for the smaller values $g_X = 10^{-11}, 10^{-12}$, but it is only barely visible in the plot given the smaller coupling. This results in a finite contribution to X shown by the step-up its energy density, and then $\nu_L^i \bar{\nu}_L^i \rightarrow X$ also becomes efficient at a later time, resulting in the bump in production of X near $T_\xi \sim 0.1$ MeV. Note that the $X \leftrightarrow e$ effective interaction rate is always positive since $m_e > m_X$ and electron-positron annihilation occurs before X decay. This means that the forward reactions ($\gamma X \rightarrow e^+e^-$ and $e^\pm X \rightarrow e^\pm \gamma$) never dominates over the backward reactions. So while electrons transfer their energy to X , the energy is never returned (unlike the case with neutrinos). This affects the evolution two-fold: (i) electron-positron annihilation dumps less entropy into photon plasma, decreasing ρ_γ ; (ii) entropy stolen from electrons/positrons is later dumped into neutrinos, further increasing ρ_ν . Both effects result in a larger value of N_{eff} .

In figure 3, we show the same plot for $m_X = 2$ MeV. In this case, the $X \leftrightarrow e^+e^-$ process is active and the population of X particles is depleted (the decays of X s) before electron-positron annihilation has completed. For $g_X = 10^{-10}$, electrons and neutrinos populate a distribution of X until $T_\xi \simeq 0.7$ MeV, then X decay takes over and dumps its entropy back into both electrons and neutrinos. However, for this mass, both e^\pm and X become non-relativistic and evolve as matter around roughly the same time. This means that the back and forth exchange in energy does not comparatively increase the energy density of electrons as it does for neutrinos. Another effect shown in figure 3 (lower) is the evolution of the effective $X \leftrightarrow e$ interaction rate from positive to negative, and then back to positive. The first positive bump is the forward reaction $e^+e^- \rightarrow X$, followed by X going nonrelativistic, with X decaying into e^+e^- and $\nu_L \bar{\nu}_L$, and then finally $e^+e^- \rightarrow X$ occurs on the Boltzmann tail of the electron distribution, and this small regenerated population of X decays mostly back into neutrinos.

In figure 4, we show the evolution for $m_X = 10$ keV with Dirac neutrinos. For low couplings, $\nu_L^i \bar{\nu}_L^i \rightarrow X$ populates X and $X \rightarrow \nu_R^i \bar{\nu}_R^i$ populates right-handed neutrinos driving $X - \nu_L - \nu_R$ system into thermal equilibrium. The energy density of primordial left-handed neutrinos is now distributed among X , ν_L , and ν_R . Hence, the maximum energy density that X can achieve is smaller than in the Majorana neutrino case. Increasing the coupling from $g_X = 10^{-12}$ to $g_X = 10^{-10}$ shows the trend towards thermalization of ν_L with ν_R as the interaction rate becomes efficient. For $g_X = 10^{-10}$, the resonance in the $X \leftrightarrow e$ system is, again, the most prominent feature in the plot. The dynamics of resonance are identical to those in figure 2. Furthermore, for $g_X = 10^{-10}$, the initial distribution of left-handed neutrinos has been converted to an equal distribution of left- and right-handed neutrinos. If this were to happen instantaneously, there would be no effect on $N_{\text{eff}} \propto (\rho_{\nu_L} + \rho_{\nu_R})/\rho_\gamma$. However, since this thermalization process generates an abundance of X , which then becomes nonrelativistic, evolves as matter, and then decays, there is an increase in N_{eff} just as occurred in the Majorana case in figure 2.

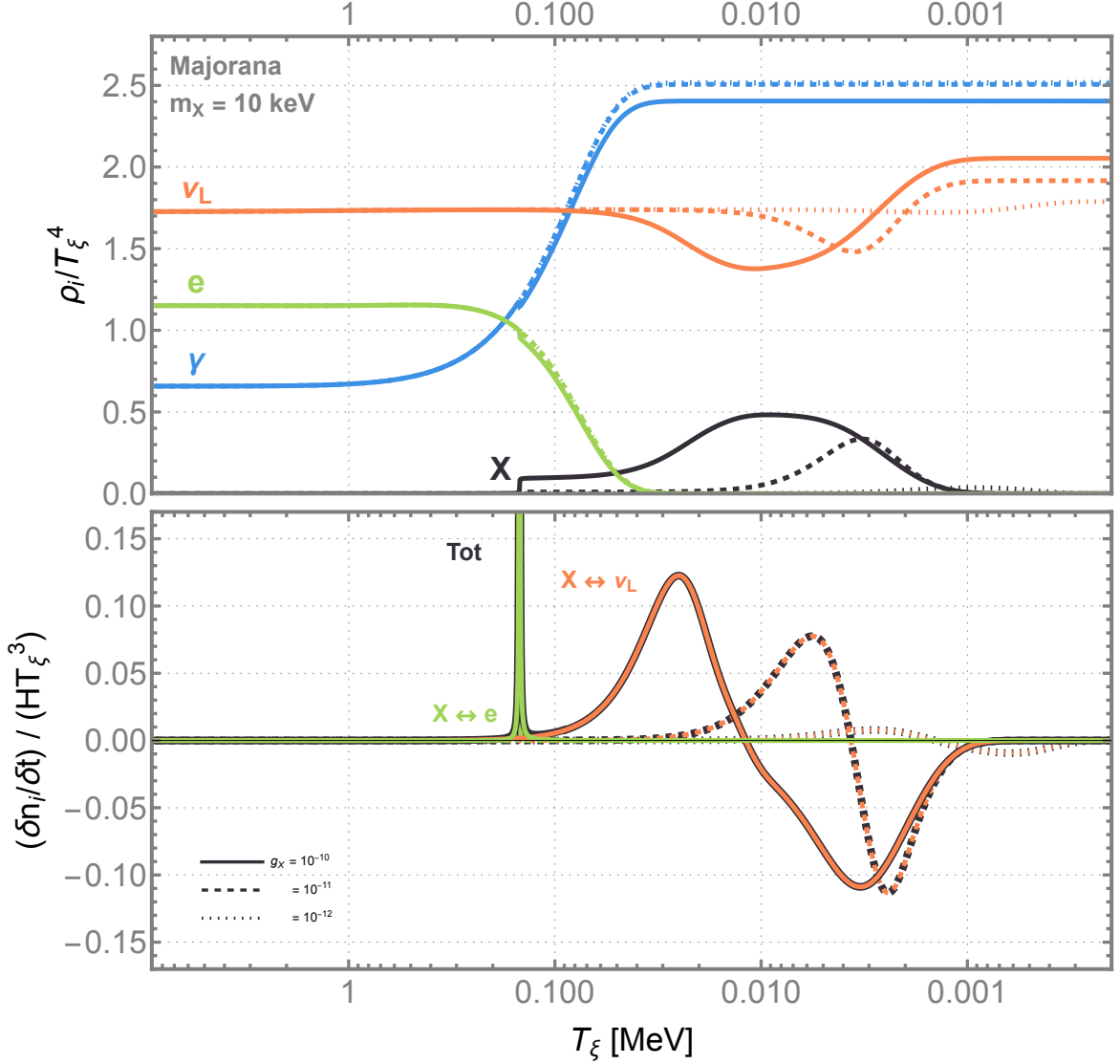


Figure 2. *Top:* The scaled density and *bottom:* and effective interaction rate for $m_X = 10$ keV for couplings $g_X = 10^{-10}$ (solid, $\Delta N_{\text{eff}} = 0.72$), $g_X = 10^{-11}$ (dashed, $\Delta N_{\text{eff}} = 0.33$), and $g_X = 10^{-12}$ (dotted, $\Delta N_{\text{eff}} = 0.08$).

5.3 Numerical results for N_{eff}

We now show the full results of our evaluation of N_{eff} in the (m_X, g_X) plane in figure 5 (Majorana neutrino case) and figure 6 (Dirac neutrino case).

Let's first discuss the Majorana neutrino case, figure 5. This is a contour plot in ΔN_{eff} , where colored regions provide our result for ΔN_{eff} as shown in the plot. In each colored region, ΔN_{eff} is greater than the value as shown, and less than its nearest neighboring region. For the dark blue region, $\Delta N_{\text{eff}} > 0.5$, and we did not delineate any larger values, for reasons that we will discuss shortly.

There are three regimes of m_X that reveal the qualitatively different processes that are occurring to determine the contribution to ΔN_{eff} . In the low mass region, $m_X < 2m_e$, with

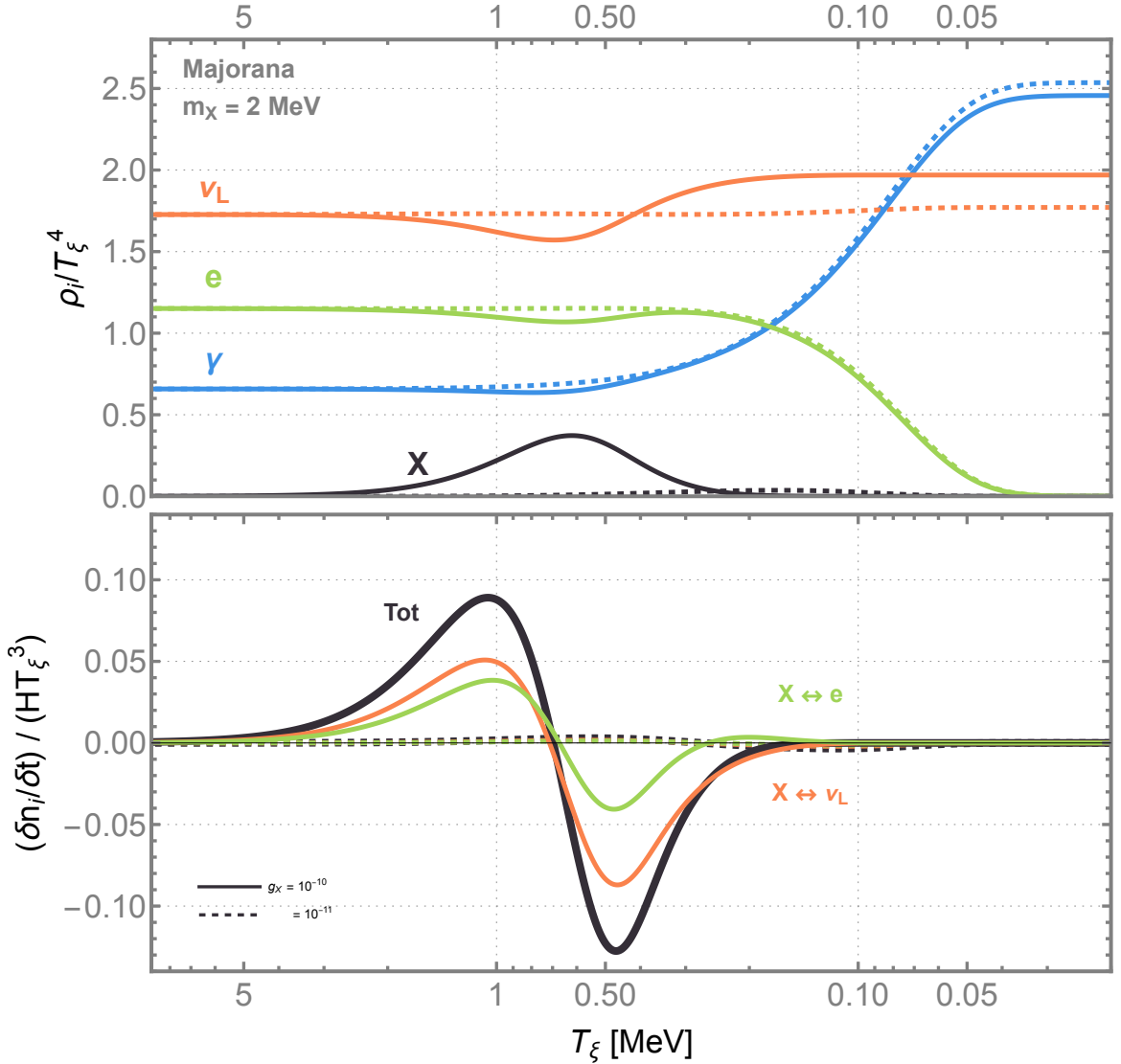


Figure 3. *Top:* The scaled density and *bottom:* and effective interaction rate for $m_X = 2$ MeV for couplings $g_X = 10^{-10}$ (solid, $\Delta N_{\text{eff}} = 0.49$) and $g_X = 10^{-11}$ (dashed, $\Delta N_{\text{eff}} = 0.03$).

$\Delta N_{\text{eff}} \sim 0.05$ to 0.2 , the process $X \leftrightarrow \nu_L \bar{\nu}_L$ is approaching thermal equilibrium. The shape of the contour in (m_X, g_X) space, $g_X \sim \sqrt{(24\pi m_X)/M_{\text{Pl}}}$, can be obtained from $\Gamma_{X \leftrightarrow \nu_L \bar{\nu}_L}/H \sim 1$ and $T = m_X$. The precise value of N_{eff} requires the numerical modeling of the Boltzmann evolution. (However, as we will see in section 6, we can also estimate the value of ΔN_{eff} using semi-analytic arguments.) We see that in this region, the bounds on g_X strengthen with *decreasing* m_X . Holding m_X fixed, as g_X is further increased, X and left-handed neutrinos reach thermal equilibrium, saturating the contribution to $\Delta N_{\text{eff}} \sim 0.3$. Once the process $X \leftrightarrow \nu_L \bar{\nu}_L$ is in thermal equilibrium, there is no further increase in ΔN_{eff} for larger values of g_X , as evident by the green plateau region in figure 5. The $\Delta N_{\text{eff}} = 0.4, 0.5$ contours, that have a different shape, arise because there are additional scattering processes that are contributing to ΔN_{eff} : the $2 \leftrightarrow 2$ processes $e^+ e^- \rightarrow X \gamma$ and $e \gamma \rightarrow e X$. These processes

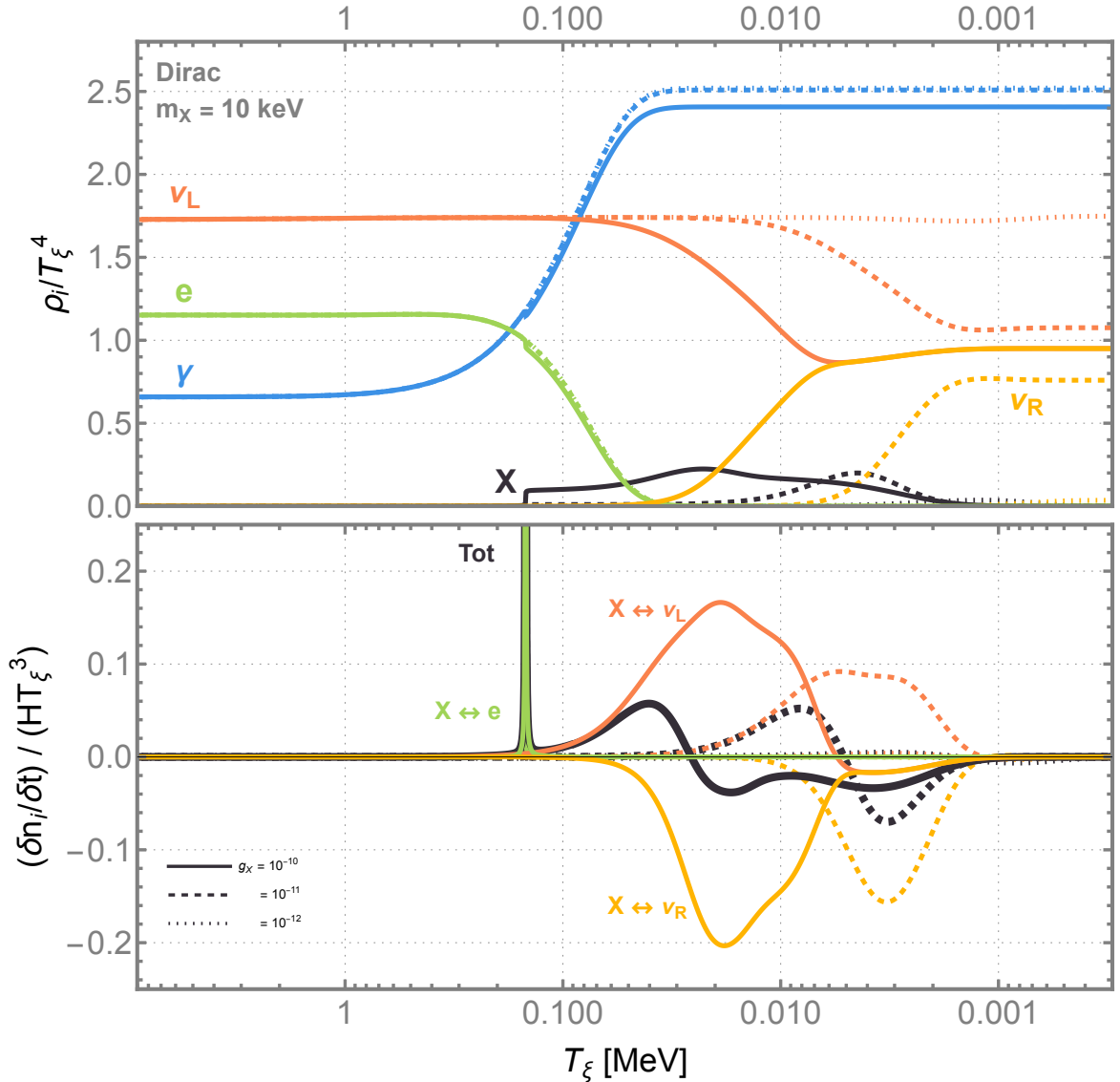


Figure 4. *Top:* The scaled density and *bottom:* and effective interaction rate for $m_X = 10$ keV with Dirac neutrinos for couplings $g_X = 10^{-10}$ (solid, $\Delta N_{\text{eff}} = 0.43$), $g_X = 10^{-11}$ (dashed, $\Delta N_{\text{eff}} = 0.18$), and in the upper figure only, $g_X = 10^{-12}$ (dotted, $\Delta N_{\text{eff}} = 0.07$).

become efficient when $n_e \langle \sigma v \rangle_{2 \leftrightarrow 2} / H \sim 1$ at $T \sim m_e$; this corresponds to couplings of order $g_X \gtrsim 10^{-10}$ if we naively treat the rates in vacuum. However, unlike $X \leftrightarrow \nu \bar{\nu}$, these processes have important finite temperature corrections⁵ that require the use of the in-medium coupling $g_{X,m}$ that is suppressed in the small m_X limit as explained in appendix B. The small kink in these contours near $m_X \sim 0.05$ MeV is the result of a linear interpolation as discussed in section 4.3.3.

In the intermediate mass region, $1 \text{ MeV} \lesssim m_X \lesssim 20 \text{ MeV}$, the contours in ΔN_{eff} rise

⁵Had finite temperature effects been neglected, the vacuum $e^+e^- \rightarrow X\gamma$ and $e\gamma \rightarrow eX$ rates are m_X independent (for $m_X \ll m_e$), and so the 0.4, 0.5 contours would have become horizontal.

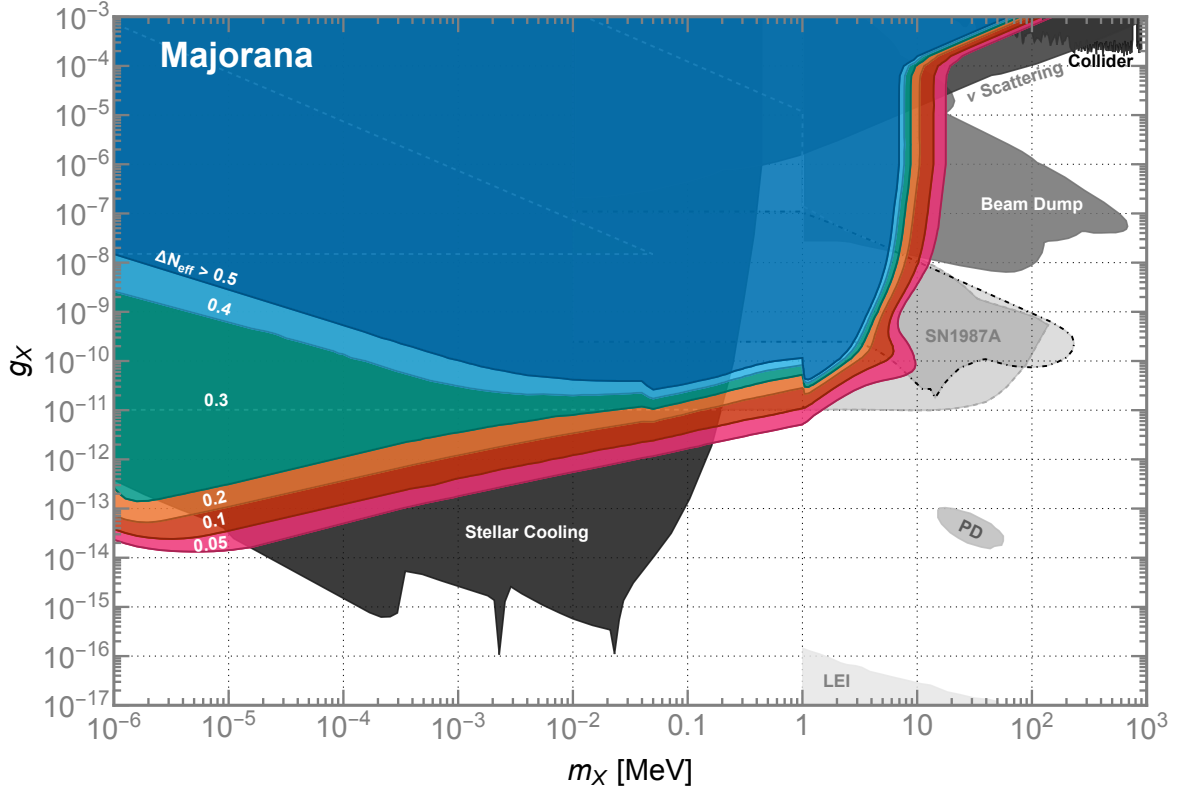


Figure 5. Calculations of ΔN_{eff} for the “Majorana” neutrino case. The regions correspond to $\Delta N_{\text{eff}} > 0.05$ (pink), 0.1 (red), 0.2 (orange), 0.3 (green), 0.4 (light blue), and 0.5 (dark blue). The dashed gray and dot-dashed black lines show the constraints from SN1987A from [93] and [94] respectively. See section 5.4 for a discussion of SN1987A and other background constraints. Current constraints from Planck data exclude $\Delta N_{\text{eff}} \gtrsim 0.3\text{-}0.4$ (depending on the choice of dataset) [26], while future CMB observatories, such as CMB-S4, are expected to reach $\Delta N_{\text{eff}} \sim 0.06$ [81]. See section 5.5 for further discussion of current and future constraints.

rapidly in g_X as m_X increases. The major contributor to the rapid rise of ΔN_{eff} contours in g_X as m_X increases is that as X becomes more massive, it becomes nonrelativistic earlier in the universe, and most of its decays back into SM matter occurs before neutrino decoupling. The SM processes rapidly equilibrate the relativistic species, erasing the effect of X production and decay. There is detailed structure, such as the shape of the contours near $\Delta N_{\text{eff}} \sim 0.05$ and masses $m_X \sim 10$ MeV, that is a more complicated interplay between X , electrons, and neutrinos.

Finally, in high mass region, $m_X > 20$ MeV, the Boltzmann evolution is calculated only involving photons, electrons, and neutrinos, with virtual X -exchange in the $2 \leftrightarrow 2$ processes $e^+e^- \leftrightarrow \bar{\nu}_\alpha\nu_\alpha$, $e^\pm\nu_\alpha \leftrightarrow e^\pm\nu_\alpha$, and $e^\pm\bar{\nu}_\alpha \leftrightarrow e^\pm\bar{\nu}_\alpha$. The ΔN_{eff} contours in this region have a shape that can be determined by requiring X -exchange is no larger than W, Z exchange. This occurs when $g_X \sim m_X\sqrt{G_F}$, providing an excellent characterization of the shape. The physics of this process is that if X exchange exceeds the weak interaction rate, this delays neutrino decoupling in the evolution of the universe, which has the effect of increasing ΔN_{eff} . Our contour shape agrees with that shown in [75].

Now, let’s discuss the contours in the Dirac neutrino case, figure 6, comparing and

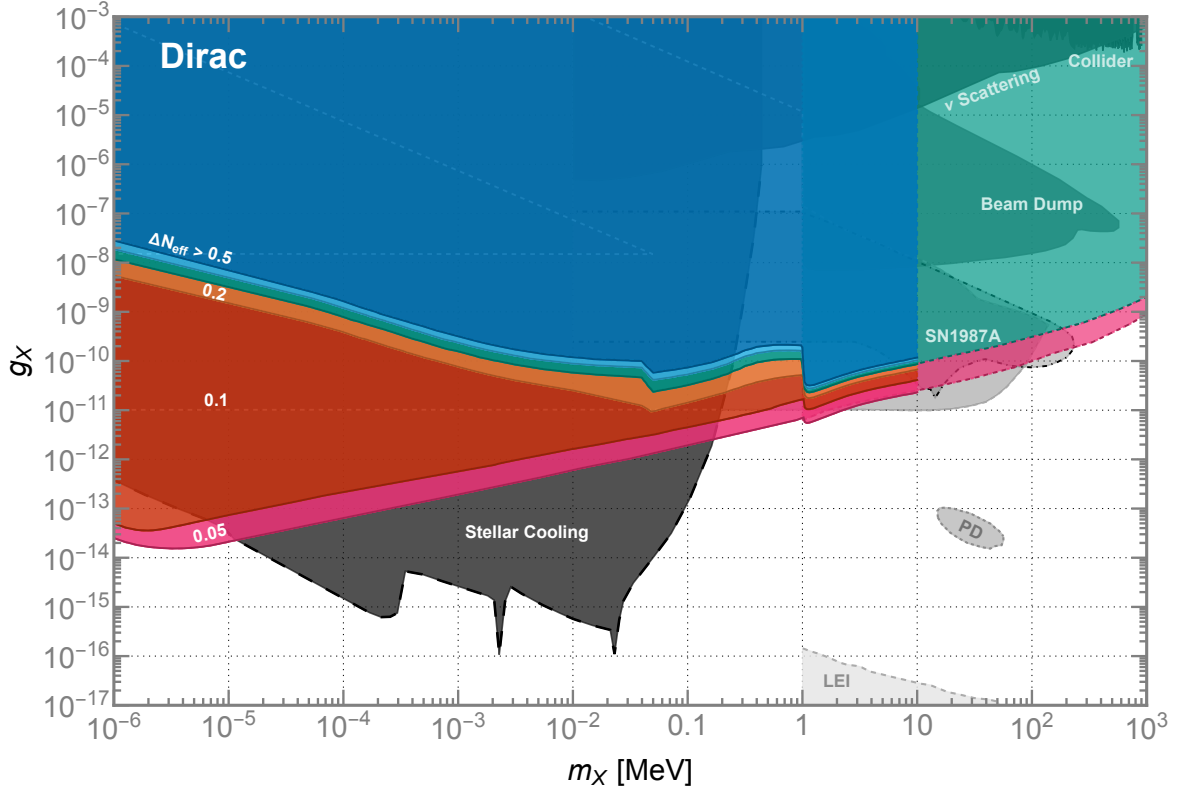


Figure 6. Same as figure 5, but for the “Dirac” neutrino case. As before, the regions correspond to $\Delta N_{\text{eff}} > 0.05$ (pink), 0.1 (red), 0.2 (orange), 0.3 (green), 0.4 (light blue), and 0.5 (dark blue). The dashed pink and green contours correspond to $\Delta N_{\text{eff}} = 0.06$ {0.3} in [67] respectively. The dashed gray and dot-dashed black lines show the constraints from SN1987A from [93] and [94] respectively. See section 5.4 for a discussion of SN1987A and other background constraints.

contrasting with the Majorana neutrino case. In the low mass region, $m_X < 2m_e$, the shape of the ΔN_{eff} contours is the same as the Majorana case, with the only difference being that the contour values of ΔN_{eff} are somewhat lower. As we discussed in section 5.2, what is happening is that the energy density of primordial left-handed neutrinos is now distributed among X , ν_L , and ν_R . Hence, the maximum energy density that X can achieve is smaller than in the Majorana case, and so the entropy dump of X into neutrinos is smaller. Later in section 6 we will verify this with a semi-analytic analysis. To be explicit, the $\Delta N_{\text{eff}} = 0.05$ contour corresponds to the $X \leftrightarrow \nu_L \bar{\nu}_L$ and $X \leftrightarrow \nu_R \bar{\nu}_R$ processes approaching equilibrium. Thermal equilibrium of these processes occurs around $\Delta N_{\text{eff}} \sim 0.1$ at which point the contribution to ΔN_{eff} from left and right handed neutrinos is saturated. We also see that at larger couplings the constraint from $e^+e^- \rightarrow X\gamma$ and $e\gamma \rightarrow eX$ processes remains, but now extends to the 0.2-0.5 contours analogous to the 0.4,0.5 contours described in the Majorana case.

At intermediate masses, $m_X \gtrsim 1$ MeV, as X is populated, then becomes nonrelativistic, it decays into both left-handed *and* right-handed neutrinos. Hence, it contributes significantly to ΔN_{eff} because X is providing a mechanism to siphon off energy density from left-handed neutrinos into a “new” species, right-handed neutrinos, that are completely decoupled from the SM. This is unlike the Majorana case, where again for $m_X \gtrsim$ few MeV, X decays

back entirely into SM states that equilibrate with the SM through electromagnetic or weak interactions. This effect of populating right-handed neutrinos implies the contours in ΔN_{eff} are at much smaller values of g_X when $m_X \gg 1$ MeV. We have calculated the result to $m_X = 10$ MeV, and then we show the contours obtained by [67] for larger masses. In particular, the dashed pink and green contours, that correspond to $\Delta N_{\text{eff}} = 0.06 \{0.3\}$, match well onto our calculations for $m_X < 10$ MeV.

There is one last issue to discuss. At the very smallest masses that we consider, the lifetime of X becomes comparable to the time of recombination

$$\tau = \frac{c}{\Gamma} \simeq 330 \text{ kyr} \times \left(\frac{1 \text{ eV}}{m_X} \right) \left(\frac{4 \times 10^{-14}}{g_X} \right)^2, \quad (5.2)$$

for the Majorana neutrino case (for the Dirac case the lifetime is 1/2 of this). This means not all of the X bosons that freeze-in have decayed back to relativistic neutrino degrees of freedom. We have taken this effect into account by evaluating N_{eff} after all of the X bosons have decayed or at the temperature of recombination, $T \simeq 0.3$ eV, whichever occurs first. This can be seen in both Figs. 5,6, where the contours of ΔN_{eff} change slope from positive to negative as m_X drops below \sim few eV, leading to slightly weaker bounds on g_X for the smallest masses of X that we consider. A very similar effect was also found in [69] for the $U(1)_{\mu-\tau}$ model.

5.4 Other constraints

In Figs. 5,6, we have also shown several other constraints on the mass and coupling of a $U(1)_{B-L}$ gauge boson. An overview of previously obtained constraints can be found from [12–15, 64].

Supernova 1987A (SN1987A) provides well-known constraints on the emission of light mediators [95]. The presence of a light vector mediator provides an additional cooling mechanism in the proto-neutron star that competes with electroweak interactions and alters its neutrino luminosity. Constraints on a variety of gauged $U(1)$ bosons have been derived in [93, 94, 96, 97]. The constraints for $U(1)_{B-L}$ in [94] and [93] are derived using slightly different methods and arrive at slightly different constraints. For completeness, we show both of these in the figures, and we will return to this issue in future work.

Similarly, constraints can be set if the energy loss rate due to light gauge boson emission from the sun, red giants (RG), and horizontal branch (HB) stars exceeds a maximally allowed limit [97–99]. Note both constraints from stellar cooling and SN1987A are derived explicitly for the case where right-handed neutrinos are heavy and do not contribute to the dynamics (“Majorana case”). To the best of our knowledge, a similar derivation has not been done in the literature for the Dirac case, though we do not suspect major differences in the results. So, we have included these constraints in figure 6, though denoted as dashed to remind the reader of this subtlety.

We also show the constraints from photodissociation (PD) of light elements, and separately, late energy injection (LEI) at the CMB era, that were obtained for $U(1)_{B-L}$ in [64]. These constraints are at much smaller coupling, where X was very far from reaching thermal equilibrium, and for masses $m_X > 2m_e$ so that the decay $X \rightarrow e^+e^-$ is kinematically available. In Figs. 5,6 we show only the upper part of the LEI contour; we refer readers to [64] for the full region that extends to couplings values $g_X < 10^{-17}$.

Neutrino experiments that probe electron-neutrino or coherent elastic neutrino-nucleus scattering (CE ν NS) are sensitive to the contribution of X to their amplitudes [100–107].

Experiments searching decays into invisible final states can also be used to set constraints with the assumption that invisible states can be treated as decays to neutrino final states [108–112]. In beam dump experiments [113–123], X is produced via the bremsstrahlung process where a beam of electron/protons is dumped on some target material; X then travels through shielding material before decaying into SM particles that can be observed in the detector. Constraints are derived by comparing the number of expected and observed events in the detector. Finally, colliders set constraints on promptly decaying X [15, 124, 125]. These beam dump and collider constraints apply to both the Majorana and Dirac case. However in the Dirac case, collider and beam dump and neutrino scattering constraints have been recast to account for the additional branching fraction of $X \rightarrow \nu_R \bar{\nu}_R$ [13].

5.5 Constraints from existing CMB observations and prospects for future observatories

We have presented our results in Figs. 5,6 with our calculated contours of ΔN_{eff} as would be measured by the CMB within the (m_X, g_X) model parameter space. Determining the current and future constraints on ΔN_{eff} requires significant care with regard to two critical issues. First, the *era* at which new physics modifies N_{eff} , and what other cosmological parameters are also modified, particularly between BBN and CMB. Second, the *datasets* used to constrain the cosmological parameters, and the potential correlations among observables. In this section, our focus is on the CMB determination of N_{eff} .

Nevertheless, we can consider two proxies for BBN constraints on new physics that are potentially different from N_{eff} . One is the helium mass fraction Y_p , that we consider in detail in section 7. A second quantity is the baryon-to-photon ratio, η . In general, new physics can contribute to a shifts in η^{CMB} relative to η^{BBN} when, for example, there is a period of late energy injection into photons well after the temperature of helium synthesis, $T \sim 0.07$ MeV [29, 126]. In the SM, there is negligible energy injection into photons at this temperature because e^+e^- annihilation is virtually complete, and so $\eta^{\text{CMB}} \simeq \eta^{\text{BBN}}$. Considering $U(1)_{B-L}$, we also do not have late energy injection directly into photons. We do have energy injection into e^+e^- from $X \rightarrow e^+e^-$, but since e^+e^- annihilation did not affect η in the SM, we do not expect these contributions from $X \rightarrow e^+e^-$ to shift η from BBN to the CMB era either.

Focusing on $N_{\text{eff}}^{\text{CMB}}$, we can now turn to the current constraints and future prospects for cosmological measurements of $N_{\text{eff}}^{\text{CMB}}$. The Planck collaboration (PCP18) have set the best bounds thus far, with various combinations of datasets [25, 26]:

$$N_{\text{eff}}^{\text{CMB}}|_{1\text{pe}}^{\text{PCP18}} = 2.99^{+0.34}_{-0.33} \quad (95\%, \text{ TT, TE, EE+lowE+ lensing+BAO}) \quad (5.3a)$$

$$N_{\text{eff}}^{\text{CMB}}|_{+Y_p}^{\text{PCP18}} = 2.99^{+0.43}_{-0.40} \quad (95\%, \text{ TT, TE, EE+lowE+ lensing+BAO+Aver [127]}) \quad (5.3b)$$

$$N_{\text{eff}}^{\text{CMB}}|_{+H_0}^{\text{PCP18}} = 3.27^{+0.30}_{-0.30} \quad (95\%, \text{ TT, TE, EE+lowE+ lensing+BAO+R18 [128]}) \quad (5.3c)$$

The first value, $N_{\text{eff}}^{\text{CMB}}|_{1\text{pe}}^{\text{PCP18}}$, is the on 1-parameter extension to the base- Λ CDM model six parameter fit. However, the primordial helium mass fraction Y_p and N_{eff} are partially degenerate as they both affect the CMB damping tail (i.e. [129]). Allowing Y_p to vary with N_{eff} gives a value of $N_{\text{eff}}^{\text{CMB}}|_{+Y_p}^{\text{PCP18}}$ and $Y_p^{\text{BBN}}|_{+Y_p}^{\text{PCP18}} = 0.2437 \pm 0.0080$ at 95% C.L.. The combined fit eases the constraint on both N_{eff} and Y_p which has a PDG recommended value of $Y_p^{\text{PDG}} = 0.245 \pm 0.006$ at 95% C.L. [30] based on the analyses in [130–134]. Finally, the $N_{\text{eff}}^{\text{CMB}}|_{+H_0}^{\text{PCP18}}$ partially addresses the $\sim 3\sigma$ tension in the Hubble constant, H_0 , between CMB and local observation determinations [128, 135, 136] by including the analysis in R18 [128].

This fit could potentially increase the tension with weak galaxy lensing and (possibly) cluster count data since it requires an increase in the σ_8 and a decrease in Ω_m values.

After the PCP18 data release and analysis, Yeh2022 [29] presents independent BBN and CMB limits on N_{eff} and η using likelihood analyses and updated evaluations for nuclear rates. The BBN likelihood functions are obtained by varying nuclear reaction rates within their uncertainties via a Monte Carlo, while the CMB likelihoods are derived from PCP18 and marginalized over Y_p . With various combinations of datasets,

$$N_{\text{eff}}^{\text{BBN}}|_{\text{BBN only}}^{\text{Yeh2022}} = 2.889 \pm 0.229 \quad (68.3\%, Y_p + \text{D}) \quad (5.4a)$$

$$N_{\text{eff}}^{\text{CMB}}|_{\text{CMB only}}^{\text{Yeh2022}} = 2.800 \pm 0.294 \quad (68.3\%, \text{TT, TE, EE+lowE+ lensing}) \quad (5.4b)$$

$$N_{\text{eff}}|_{\text{BBN+CMB}}^{\text{Yeh2022}} = 2.898 \pm 0.141 \quad (68.3\%, \text{TT, TE, EE+lowE+ lensing} + Y_p + \text{D}). \quad (5.4c)$$

The first value, $N_{\text{eff}}^{\text{BBN}}|_{\text{BBN only}}^{\text{Yeh2022}}$, shows limits on N_{eff} at BBN where the BBN likelihood is convolved with the observation determination of Y_p and deuterium abundance D [137–144] likelihoods. The second value, $N_{\text{eff}}^{\text{CMB}}|_{\text{CMB only}}^{\text{Yeh2022}}$, differs from equation (5.3a) as the Yeh2022 analysis does not assume any relation between the ^4He abundance and the baryon density. The third value is the limit set by combining BBN and the CMB assuming no new physics after nucleosynthesis, however this value is not applicable here since X interactions can affect ΔN_{eff} between BBN and CMB.

Comparing these observations to our results, Figs. 5,6, a conservative analysis suggests $\Delta N_{\text{eff}}^{\text{CMB}} \lesssim 0.3\text{--}0.4$ to 95% C.L., and hence the regions labeled dark and light blue are ruled out, with the green region strongly disfavored. The 2018 Planck analysis that incorporated the local Hubble measurement into the fit yielded $N_{\text{eff}}^{\text{CMB}} \simeq 3.27$, Eq. (5.3c), which would favor the orange region, however this is in tension with more recent analyses of the CMB data. If the ultimate resolution of the Hubble tension involves a slightly larger value of equation (5.3c), then the orange region is favored. Future observatories, including SPT-3G [145], CORE [146], Simons Observatory [147], PICO [148], CMB-S4 [81], CMB-HD [149], are anticipated to reach much smaller values, for example CMB-S4 is anticipated to ultimately obtain $\Delta N_{\text{eff}} \simeq 0.06$ at 95% C.L. [81]. Here we see these future experiments are capable of probing a significantly larger fraction of the (m_X, g_X) parameter space in both the Majorana and Dirac neutrino cases. The future CMB observations will be the most sensitive to the presence of a gauged $U(1)_{B-L}$ boson in the regions $1 \text{ eV} \lesssim m_X \lesssim 20 \text{ eV}$, $0.2 \text{ MeV} \lesssim m_X \lesssim 20 \text{ MeV}$, and in the Dirac case, $m_X \gtrsim 200 \text{ MeV}$ [67].

6 Semi-analytic estimates of ΔN_{eff}

There is an interesting way to cross-check our results in the regime $m_X \ll m_e$, where the only interactions of X are with neutrinos. This semi-analytic approach involves two steps. First, we calculate the energy densities and number densities of X , assuming thermalization occurs at a temperature $T > m_X$. For the purposes of this estimate, we assume that thermalization occurs when X is relativistic and can be treated as massless. The key nontrivial part of this first step is that we are solving for not only the energy densities but also the chemical potentials as X is frozen-in to equilibrium with neutrinos. Next, we use entropy conservation to determine the net effect of X decaying back into neutrinos. Again, this step is nontrivial because we also must take into account the nonzero chemical potentials of X and the various neutrino species that (were) in equilibrium.

Given these assumptions, we are able to semi-analytically calculate the contribution to ΔN_{eff} . We now present the calculation in two regimes: first, the Majorana case, to get a clear sense of the method and its result. Next, the Dirac case, however we will generalize this to include an arbitrary number of additional species of (right-handed) fermions that carry lepton number. This case will allow us to provide semi-analytic estimates of ΔN_{eff} in a wider range of models that may be relevant for dark matter and cosmology.

6.1 Majorana case

An initial density of left-handed neutrinos with temperature T_{ν_L} is converted to a density of left-handed neutrinos and X ,

$$\rho_{\nu_L}(T_{\nu_L}, 0) = \rho_{\nu_L}(T_{\text{eq}}, \mu_{\text{eq}}) + \rho_X(T_{\text{eq}}, 2\mu_{\text{eq}}) \quad (6.1a)$$

$$n_{\nu_L}(T_{\nu_L}, 0) = n_{\nu_L}(T_{\text{eq}}, \mu_{\text{eq}}) + 2n_X(T_{\text{eq}}, 2\mu_{\text{eq}}), \quad (6.1b)$$

with $T_{\text{eq}}, \mu_{\text{eq}}$ thermal equilibrium temperature and chemical potential. In the second equation, the factor of 2 arises because one X is produced at the expense of two neutrinos in $\nu_L^i \bar{\nu}_L^i \rightarrow X$. These conditions give,

$$T_{\text{eq}} = 1.208 T_{\nu_L}, \quad \mu_{\text{eq}} = -1.166 T_{\nu_L} \quad (6.2)$$

which gives a maximum density ratio $\varrho_X \equiv \rho_X/(\rho_{\nu_L} + \rho_X) = 0.1642$. Had we neglected chemical potential, equation (6.1a) becomes a degree of freedom counting argument which yields $\varrho_X = 3/(6 \times \frac{7}{8} + 3) = \frac{4}{11} = 0.3636$ significantly overestimating the maximum X abundance. Instead, the chemical potential appears as $\varrho_X = 3 \text{Li}_4(x)/[6 \text{Li}_4(-x) + 3 \text{Li}_4(x)]$ with $x \equiv e^{\mu/T}$ and Li_4 is the 4th order polylogarithm.

After thermal equilibrium is reached, we use entropy conservation to write,

$$[s_{\nu_L}(T_{\text{eq}}, \mu_{\text{eq}}) + s_X(T_{\text{eq}}, 2\mu_{\text{eq}})] a'^3 = s_{\nu_L}(T_\nu, \mu_\nu) a^3 \quad (6.3a)$$

$$[n_{\nu_L}(T_{\text{eq}}, \mu_{\text{eq}}) + 2n_X(T_{\text{eq}}, 2\mu_{\text{eq}})] a'^3 = n_{\nu_L}(T_\nu, \mu_\nu) a^3. \quad (6.3b)$$

The left-hand side starts at scale factor a' with equilibrium abundance of all relevant particles, while the right-hand side ends at a scale factor a with $T_\nu \ll m_X$, where the entire distribution of X bosons has decayed into neutrinos. We can relate the scale factors through $T'_\gamma a' = T_\gamma a$, since the photon plasma is decoupled from neutrinos. Solving equation (6.3) gives,

$$T_\gamma/T_\nu = 1.278, \quad T_\nu/\mu_\nu = -3.486 \quad (6.4)$$

which can be used to calculate

$$\Delta N_{\text{eff}} = N_{\text{eff}} - N_{\text{eff}}^{\text{SM}} = 0.25. \quad (6.5)$$

As we discussed in section 5.3, the diagonal contours of ΔN_{eff} in the light regime $m_X \ll 2m_e$ correspond to when the $1 \leftrightarrow 2$ process $X \leftrightarrow \nu\bar{\nu}$ approximately reaches thermal equilibrium. The highest contour shown is 0.3, that is quite close to our semi-analytic estimate in equation (6.5). Of course the semi-analytic method required certain approximations to be taken. Namely, in solving equation (6.3) we used the SM value of T_γ/T_ν in equation (3.2) to relate the scale factors $T'_\gamma a' = T_\gamma a$; and using the numerical value obtained by solving the Boltzmann equations in equation (4.3) reproduces the correct value of ΔN_{eff} .

6.2 Dirac and generalized cases

We now redo the analysis of section 6.1 by adding into the thermal bath an arbitrary number N_R of (Weyl) fermion species.⁶ As a slight abuse of notation, we will refer to these fermions as “right-handed neutrinos” below, but it should be understood that these fermion fields have $L = \pm 1$ and may or may not pair up with the left-handed neutrinos to gain Dirac masses. All of these right-handed neutrinos will be considered to be either (i) massless, or (ii) having a mass $m_{\nu_R} \lesssim m_X/2$. The Dirac case follows as a special case of this generalization where $N_R = 3$, $m_{\nu_R} = 0$, and two (or three) of these fermion species pair up with left-handed neutrinos.

Following Eqs. (6.1), an initial density of left-handed neutrinos with temperature T_{ν_L} is converted to a energy (number) density of left- and right-handed neutrinos [denote collectively by ρ_ν (n_ν)⁷ and X ,

$$\rho_{\nu_L}(T_{\nu_L}, 0) = \left(1 + \frac{N_R}{3}\right) \rho_\nu(T_{\text{eq}}, \mu_{\text{eq}}) + \rho_X(T_{\text{eq}}, 2\mu_{\text{eq}}) \quad (6.6a)$$

$$n_{\nu_L}(T_{\nu_L}, 0) = \left(1 + \frac{N_R}{3}\right) n_\nu(T_{\text{eq}}, \mu_{\text{eq}}) + 2n_X(T_{\text{eq}}, 2\mu_{\text{eq}}) \quad (6.6b)$$

with $T_{\text{eq}}, \mu_{\text{eq}}$ thermal equilibrium temperature and chemical potential.

After thermal equilibrium is reached, we can again utilize entropy conservation to write,

$$\left[\left(1 + \frac{N_R}{3}\right) s_\nu(T_{\text{eq}}, \mu_{\text{eq}}) + s_X(T_{\text{eq}}, 2\mu_{\text{eq}}) \right] a'^3 = \left[\left(1 + \frac{N_R}{3}\right) s_\nu(T_\nu, \mu_\nu) \right] a^3 \quad (6.7a)$$

$$\left[\left(1 + \frac{N_R}{3}\right) n_\nu(T_{\text{eq}}, \mu_{\text{eq}}) + 2n_X(T_{\text{eq}}, 2\mu_{\text{eq}}) \right] a'^3 = \left[\left(1 + \frac{N_R}{3}\right) n_\nu(T_\nu, \mu_\nu) \right] a^3. \quad (6.7b)$$

Again, the left-hand side starts at scale factor a' with equilibrium abundance of all relevant particles and the right-hand side ends at scale factor a with $T_\nu \ll m_X$ where all X distribution has decayed into neutrinos.

6.2.1 Dirac case

In the Dirac case ($N_R = 3$; $m_{\nu_R} = 0$), Eqs. (6.6) give

$$T_{\text{eq}} = 1.1088 T_{\nu_L}, \quad \mu_{\text{eq}} = -1.3485 T_{\nu_L} \quad (\text{Dirac case}) \quad (6.8)$$

which gives a maximum density ratio $\varrho_X \equiv \rho_X/(\rho_{\nu_L} + \rho_X + \rho_{\nu_R}) = 0.07049$. (Again, had we neglected chemical potential, equation (6.6a) becomes $\varrho_X = 3/(12 \times \frac{7}{8} + 3) = \frac{2}{9} = 0.2222$, overestimating the maximum X abundance.) Solving equation (6.7) gives,

$$T_\nu/T_{\nu_L} = 1.322, \quad T_\nu/\mu_\nu = -1.093 \quad (\text{Dirac case}) \quad (6.9)$$

which can be used to calculate

$$\Delta N_{\text{eff}} = N_{\text{eff}} - N_{\text{eff}}^{\text{SM}} = 0.09. \quad (6.10)$$

⁶Here N_R refers to the number of $L = \pm 1$ particles, and so not necessarily are they are strictly “right-handed” with $L = 1$. The Dirac case has $N_R = 3$ and $L = 1$ for all species. The sign of the lepton number of any of these species does not enter our discussion below.

⁷Note that both quantities ρ_ν and n_ν include a factor of $g_\star = 6$ corresponding to three fermionic Weyl degrees of freedom in their definition.

Like our discussion above in the Majorana case, in figure 6 the highest contour consistent with approximate thermalization of $X \leftrightarrow \nu\bar{\nu}$ is 0.1, that agrees with the semi-analytic estimate in equation (6.10).

6.2.2 Large number of massless species

Now let's utilize the generalized results in Eqs. (6.6) and (6.7) to apply to the case where there is a large number of massless species $N_R \gg 1$ that X can decay into. Once X and the $1 + N_R/3$ neutrinos have thermalized, it is clear from Eqs. (6.6) that the energy and number density of X is suppressed by the same factor, $1/(1 + N_R/3)$. Most of the energy and number density of left-handed neutrinos is transferred into the larger number of right-handed neutrinos. Then, following Eqs. (6.7), the effect of the small number of X gauge bosons is negligible. That is, in the limit $N_R \gg 1$, there is negligible entropy dumping of X into neutrinos, and so $\Delta N_{\text{eff}} \rightarrow 0$. For smaller values of N_R , we find, for example $\Delta N_{\text{eff}} = 0.12$ ($N_R = 2$), $\Delta N_{\text{eff}} = 0.07$ ($N_R = 4$) and $\Delta N_{\text{eff}} = 0.03$ ($N_R = 8$). Here we do need to emphasize that while the number of relativistic degrees of freedom nearly matches the SM, the *flavor* of these degrees of freedom is overwhelmingly in the form of the (sterile) neutral fermion species carrying lepton number.

6.2.3 Massive species

An alternative scenario occurs if the N_R species are massive, and thus are able to annihilate through X back into (massless) left-handed neutrinos species. Here what happens is that the large entropy of the right-handed neutrinos siphons off virtually all of the entropy in left-handed neutrinos. In the limit $N_R \gg 1$, with $m_{\nu_R} \lesssim m_X/2$, the overwhelming majority of the original energy density of left-handed neutrinos end up as nonrelativistic, massive (sterile) neutral fermion species. This leaves a negligible amount of left-handed neutrinos, and so in this limit, $\Delta N_{\text{eff}} \rightarrow -3$, i.e., $N_{\text{eff}} \rightarrow 0$. As a few examples where all N_R species are massive, we find $\Delta N_{\text{eff}} = -0.64$ ($N_R = 1$), $\Delta N_{\text{eff}} = -1.15$ ($N_R = 2$) and $\Delta N_{\text{eff}} = -1.48$ ($N_R = 3$). Notice that $N_R \geq 1$ is already completely excluded by the Planck constraints on the CMB, i.e., equation (5.3).

7 BBN Y_p

The primordial abundances of nuclide species are critically sensitive to the expansion history leading up to nucleosynthesis. Precise determinations of these abundances requires solving Boltzmann equations describing the density evolution of each nuclide species (^2H , ^3He , ^4He ...) (i.e. [47]). This can be done using publicly available BBN code such as `PARthENoPE` [150, 151], `AlterBBN` [152, 153], `PRIMAT` [154], or `PRyMordial` [155]; however, this is beyond the scope of this paper.

Instead, we follow an approximation employed in appendix A.4 of [60], that involves modifying the neutron-to-proton conversion rate to include a neutrino chemical potential following the derivation in [34, 36]. The Boltzmann equation describing the evolution of

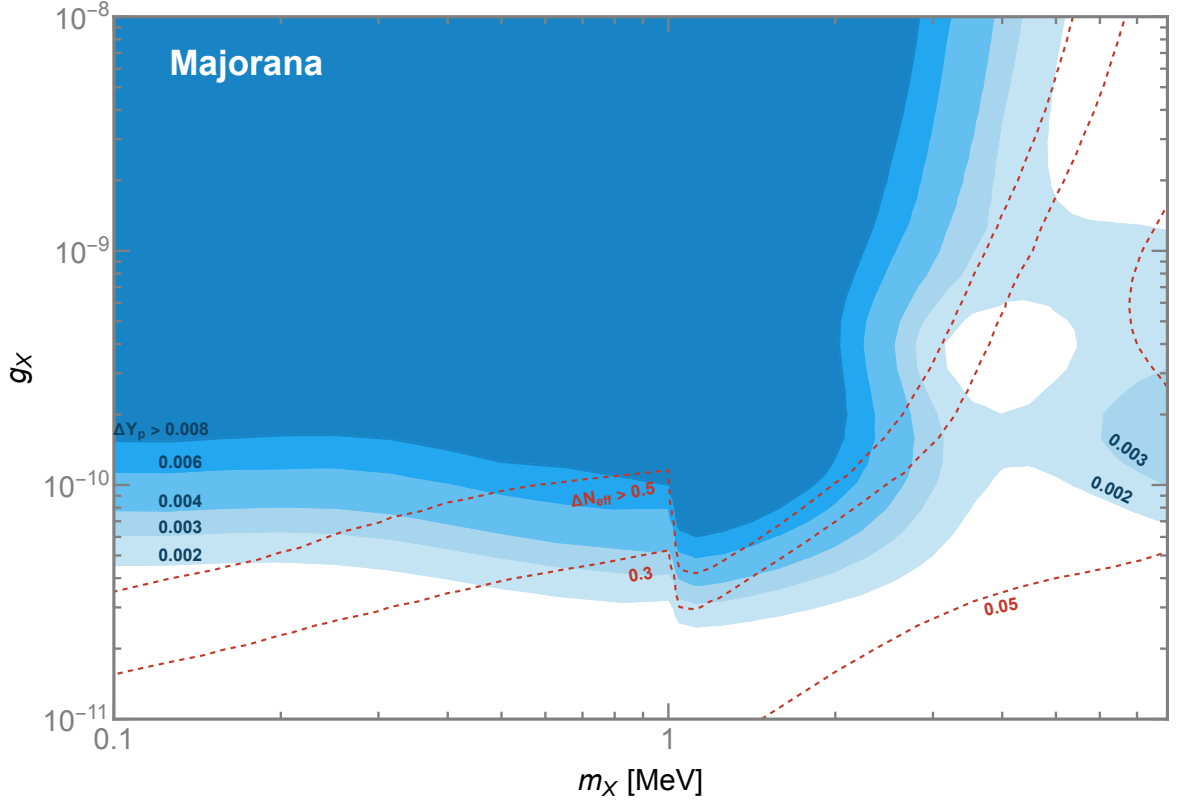


Figure 7. ΔY_p contours for “Majorana” neutrino case. The dashed red lines show the contours from our calculation of ΔN_{eff} observed by the CMB, from figure 5. A conservative upper bound is $\Delta Y_p = 0.008$ at 95% C.L. [29], see section 7 for further discussion.

neutron fraction $X_n = \frac{n_n}{n_n + n_p}$ is [46]:

$$\frac{dX_n}{dt} = \Gamma_{pn}(1 - X_n) - \Gamma_{np}X_n, \quad (7.1a)$$

$$\Gamma_{np} = K \int_1^\infty d\epsilon \left[\frac{(\epsilon - q)^2(\epsilon^2 - 1)^{1/2}\epsilon}{(1 + e^{-\epsilon z_\gamma})(1 + e^{(\epsilon - q - \tilde{\mu}_\nu)z_\nu})} + \frac{(\epsilon + q)^2(\epsilon^2 - 1)^{1/2}\epsilon}{(1 + e^{\epsilon z_\gamma})(1 + e^{-(\epsilon - q - \tilde{\mu}_\nu)z_\nu})} \right], \quad (7.1b)$$

$$\Gamma_{pn} = \Gamma_{np}(-q), \quad (7.1c)$$

where $z_i = m_e/T_i$, $\tilde{\mu}_\nu = \mu_\nu/m_e$, $q = (m_n - m_p)/m_e$, and $K \simeq (1.939\tau_n)^{-1}$. We take $m_n - m_p = 1.2933$ MeV and neutron lifetime $\tau_n = 878.4$ s [30]. Here Γ_{np} is the rate for neutron to proton conversion through the weak interactions $n + \nu_e \leftrightarrow p + e^-$, $n + e^+ \leftrightarrow p + \bar{\nu}_e$, and $n \leftrightarrow p + e^- + \bar{\nu}_e$. The evolution of T_γ , T_ν and μ_ν are obtained separately, by solving equation (4.3) as described in section 4.2. To estimate the helium abundance Y_p , we take the limit where all remaining neutrons form helium around the temperature where photons no longer dissociate deuterium $T_D = 0.073$ MeV; in other words,

$$Y_p \simeq 2X_n|_{T=T_D}. \quad (7.2)$$

In the SM, applying this procedure yields $Y_p|_{\text{SM}}^{\text{equation 7.2}} = 0.248$ in agreement with $Y_p|^{\text{PDG}} = 0.245 \pm 0.006$ at 95% C.L. [30]. We define the BSM deviation of helium abundance

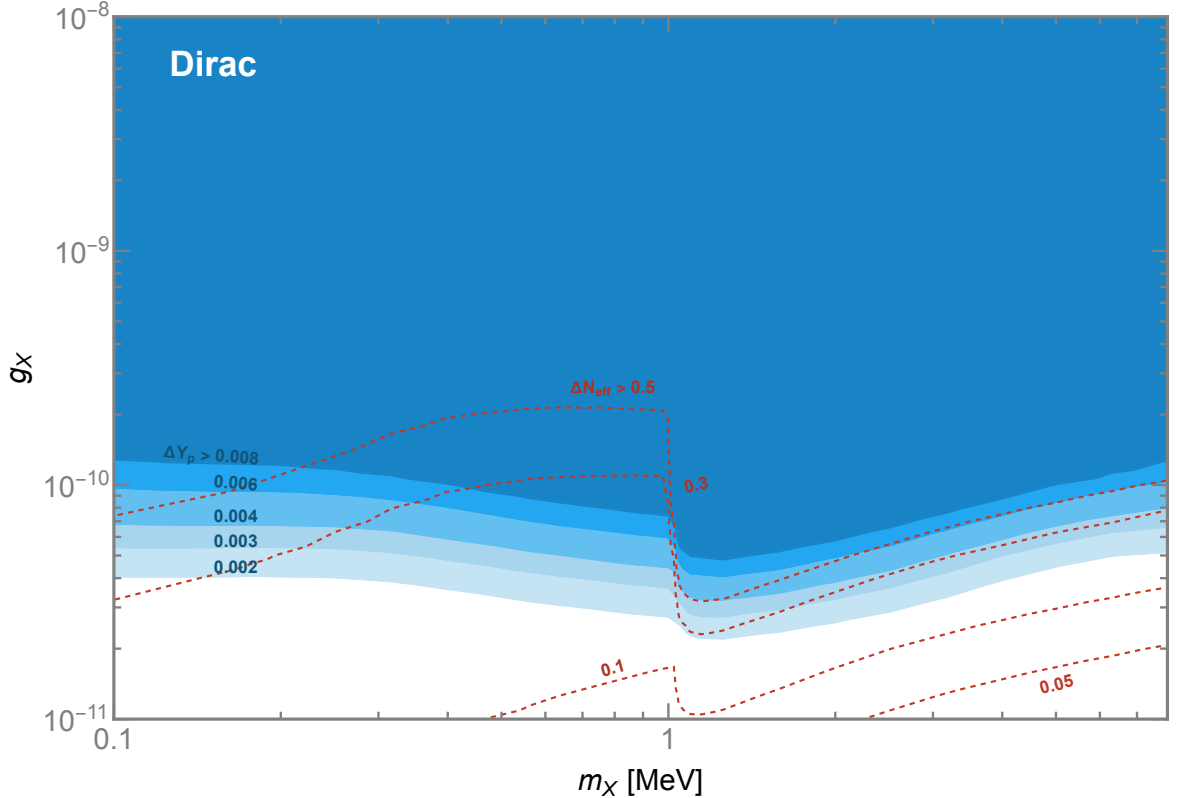


Figure 8. Same as figure 7, but for the “Dirac” neutrino case. The dashed red lines show the contours from our calculation of ΔN_{eff} observed by the CMB, from figure 6.

as

$$\Delta Y_p = Y_p|_{\text{BSM}}^{\text{equation 7.2}} - Y_p|_{\text{SM}}^{\text{equation 7.2}}. \quad (7.3)$$

The ΔY_p contours for the Majorana and Dirac case are shown in Figs. 7,8, along with overlays of the respective ΔN_{eff} contours in red. In accordance with the discussion in section 5.5, a conservative upper bound is $\Delta Y_p = 0.008$ at 95% C.L. In both the Majorana and Dirac cases, ΔN_{eff} constraints are stronger for $m_X > 2m_e$. However, in the Dirac case, we find $\Delta Y_p \gtrsim 0.008$ in the mass region $0.3 \text{ MeV} \lesssim m_X \lesssim 2m_e$, where the Planck constraint from the CMB, $\Delta N_{\text{eff}} \lesssim 0.3$ is currently weaker. Once the future CMB observatories reach $\Delta N_{\text{eff}} \lesssim 0.15$, their constraints will exceed what can be set by this analysis of BBN.

8 Discussion

In this paper we calculated the contributions of a light $U(1)_{B-L}$ gauge boson mediator to ΔN_{eff} as measured by the CMB and Y_p from BBN. Our main result is Figs. 5,6, where we show our predictions for ΔN_{eff} as a function of of the $U(1)_{B-L}$ gauge boson mass m_X and coupling strength g_X , along with Figs. 7,8 where we show our predictions for the shift in the helium mass fraction ΔY_p , in the same parameter space. While substantial portions of the (m_X, g_X) parameter space have overlapping constraints from other astrophysical or terrestrial experiments, we find there are several regions where future CMB observatories [81, 145–149], have the opportunity to gain sensitivity to a very weakly coupled $U(1)_{B-L}$ gauge boson in certain mass and coupling ranges that is not accessible by any other method.

We have also calculated ΔY_p , the helium abundance, which serves as a proxy for ΔN_{eff} as observed by BBN. This result utilized an approximation from Ref. [60] to estimate the change in the helium abundance that follows from a nonzero neutrino chemical potential, as occurs with a freeze-in abundance of a $U(1)_{B-L}$ gauge boson. In figure 7, we find that for the Majorana case, the Planck constraints on the CMB are generally stronger than the BBN constraints on Y_p throughout the (m_X, g_X) plane. For the Dirac case shown in figure 8, however, there is a nontrivial region of parameter space (approximately $0.3 \text{ MeV} \lesssim m_X \lesssim 1 \text{ MeV}$, $g_X \lesssim 10^{-10}$), where the BBN constraints are stronger than the constraints from ΔN_{eff} from Planck data. However, future CMB observatories [81, 145–149], will be able to fully cover this region, and probe considerably smaller couplings, once they achieve $\Delta N_{\text{eff}} \lesssim 0.1$ sensitivity.

It is interesting to consider whether thermal equilibrium is ever achieved between X and the SM. In general, for large enough couplings, there will be an epoch where we can identify equilibrium. This occurs when the comoving energy densities of X and one or more SM species reach approximately constant values. This epoch cannot last forever, since X subsequently decays back into the SM. For example, in figure 2 where $m_X = 10 \text{ keV}$, X clearly reaches thermal equilibrium with neutrinos when $g_X = 10^{-10}$, as shown by the plateau of the energy density for a finite range of temperature. The next contour, $g_X = 10^{-11}$, there is hardly any range of temperature where the X density remains constant, and so we see that for this coupling, X approaches thermal equilibrium with neutrinos but never really achieves this before X subsequently decays. Similar results can also be found for the Dirac case, comparing $g = 10^{-10}$ to $g = 10^{-11}$ in figure 4. In the region $m_X \ll 2m_e$, broadly we find that X and neutrinos approximately achieve thermal equilibrium, for a brief point in the temperature evolution of the universe, in the $\Delta N_{\text{eff}} \sim 0.3$ (green) region in figure 5 and the $\Delta N_{\text{eff}} \sim 0.1$ (red) region in figure 6.

We also considered semi-analytic estimates of our ΔN_{eff} results. Our focus for these estimates was the region $m_X \ll 2m_e$, where the only species interacting with X are neutrinos. The semi-analytic estimates, which assume thermal equilibrium is reached between X and neutrinos, allow us to obtain an approximate value for $\Delta N_{\text{eff}} \simeq 0.25$ (0.09) for the Majorana (Dirac) case. The semi-analytic estimates also permit us to determine how our results change if there are additional degrees of freedom, beyond the SM, that the X boson is able to populate. The physical picture is that X slowly freezes in, becomes nonrelativistic, and then decays into SM states plus the additional degrees of freedom beyond the SM. For this analysis, we considered a set N_R of fermions carrying lepton number (right-handed neutrinos with $L = \pm 1$), in two scenarios: the additional fermions stay relativistic (at least until recombination), or the additional fermions have masses and become nonrelativistic matter. If the fermions stay relativistic, $\Delta N_{\text{eff}} \rightarrow 0$ as N_R becomes large, essentially because they dominate the relativistic degrees of freedom after entropy equilibration. On the other hand, if they become nonrelativistic before recombination, they siphon off most of the relativistic degrees of freedom into matter, and so $N_{\text{eff}} \rightarrow 0$ ($\Delta N_{\text{eff}} \rightarrow -3$).

Our results have interesting implications on other scenarios considered in the literature:

Ref. [156] considered light new vectors produced gravitationally during inflation that also couple to neutrinos. The coupling to neutrinos imply the inflationary produced vector can decay into neutrinos, giving additional contributions to ΔN_{eff} , that led to constraints in the (m_X, g_X) plane. These contributions to ΔN_{eff} rely on a primordial abundance of vector bosons from inflation, and thus constitute a contribution that is *in addition* to the freeze-in abundance of a massive vector that couples to neutrinos. On comparing our bounds to those

from [156], we find our constraints would appear to place significant restrictions on the scale of inflation and hence the inflationary production of vector bosons that couple to neutrinos.

One of the additional effects of a light X boson, with a mass well below the neutrino decoupling temperature, $m_X \ll 2$ MeV, is that the interactions with X can suppress the free streaming of neutrinos, and this has independent constraints from the suppression of small scale structure [157] that results in shifts in the phase and a decrease in the amplitude of the acoustic peaks of the CMB [57, 158–160]. Recently, [69] analyzed the suppression of neutrino free streaming resulting from neutrino interactions within the context of a model with a very light $U(1)_{\mu-\tau}$ gauge boson. By implementing these interactions into the modeling of the CMB, they were able to use Planck data to constrain a broad range of $U(1)_{\mu-\tau}$ gauge boson masses between 10^{-3} eV to 10^3 eV, with the strongest bound on $g_{\mu-\tau}$ near 1 eV, and rapidly decreasing bounds as the mass moved away from this value. Nevertheless, for masses 1 eV and larger, [69] found that the bounds from ΔN_{eff} are still stronger than those from the suppression of the free streaming of neutrinos. This is strongly suggestive that the bounds from ΔN_{eff} are very likely stronger than constraints from the suppression of neutrino free streaming in the model considered in this paper, $U(1)_{B-L}$, though we leave a detailed analysis of this point to future work.

Several other papers have considered a light $U(1)_{B-L}$ gauge boson’s effects in various contexts. For example, our work complements and extends the analysis of [13, 61, 66, 67], who considered bounds on a $U(1)_{B-L}$ model in which neutrinos acquire Dirac masses. Our work rules out substantial parts of previously allowed parameter space in [161], who considered constraints on $U(1)_{B-L}$ from neutrino-electron and neutrino-nucleon scattering. As can be seen in figure 5, the remaining region that is more strongly constrained by neutrino-nucleon scattering occurs only when $m_X \gtrsim 10$ MeV in the Majorana case. By contrast, when neutrinos have Dirac masses, the CMB constraints completely dominate the bounds even at larger masses as shown in figure 6 (that includes the results from [67]). Some groups [68, 162–164] considered sterile neutrino dark matter arising from interactions with $U(1)_{B-L}$. While our analysis of the CMB constraints does not rule out the main region favored by [164], essentially all of their parameter space $m_X \lesssim 10$ MeV would be in conflict with the CMB that extends and compliments the existing constraints from beam dump experiments. Ref. [68] calculated CMB constraints in the range 0.001 MeV $< m_X < 1$ MeV, and while the broad trends they find in their paper are similar with our Majorana case results, they did not include a chemical potential for X and neutrinos, making a quantitative comparison moot.

Beyond $U(1)_{B-L}$, there has also been extensive discussion of equilibration of a dark sector with neutrinos well after BBN [126, 165, 166]. The motivation of this work is to obtain thermal dark matter below an MeV [165, 166]. There are commonalities between this work and ours, specifically the observation that if a light state couples only to neutrinos, equilibration with neutrinos draws heat from the SM, and only after the species decouples, the neutrino bath is heated, contributing to ΔN_{eff} . The distinction between our work and [126, 165, 166] is that we find the Boltzmann equations require the presence of a nonzero chemical potential for X as well as neutrinos, in order to properly track the evolution of the energy densities of the various species, and therefore to accurately calculate ΔN_{eff} . For instance, when our X boson can decay into just one massive species (one massive “sterile” Majorana neutrino), this siphons off a sufficient amount of entropy from the left-handed neutrinos of the SM to already be excluded by Planck data. It would be very interesting to apply our analysis to the specific scenarios of [165, 166], to determine if including a chemical potential for the mediators and DM has an effect on the results, but we leave for future work.

Note added: As this work was being completed [167] appeared that also discussed the bounds on a model with a light $U(1)_{B-L}$ (with Majorana neutrino masses) and $U(1)_{\mu-\tau}$ boson from ΔN_{eff} . Among the differences between their work and ours, we include the coupling of the $U(1)_{B-L}$ mediator to charged leptons (electrons), and the associated $1 \leftrightarrow 2$, $2 \leftrightarrow 2$ processes that are essential to determining the effects on ΔN_{eff} for temperatures near and above BBN.

Acknowledgments

We thank P. Asadi, M. Dolan, M. Escudero, and J. Kopp for useful discussions. This work was supported in part by the U.S. Department of Energy under Grant Number DE-SC0011640.

A Right-handed neutrino decay in Majorana case

In the regime $M_R > m_h + m_\nu$, the 2-body decay is rapid, and the right-handed neutrinos will have completely decayed well prior to BBN. When $M_R < m_h$, the decay is 3-body, with an off-shell Higgs that will also be suppressed by the small Yukawa coupling y_{SM} of the Higgs to lighter SM fermions. An estimate of this 3-body width to one SM fermion pair is sufficient for our purposes,

$$\Gamma(\nu_R \rightarrow \nu_L f \bar{f}) \sim \frac{y_D^2 y_{\text{SM}}^2 M_R^5}{128\pi^3 m_h^4}, \quad (\text{A.1})$$

where we have neglected the final state phase space. If a SM neutrino species has a mass $m_\nu \sim (y_D v)^2/M_R$, the width becomes

$$\Gamma(\nu_R \rightarrow \nu_L f \bar{f}) \sim \frac{m_\nu y_{\text{SM}}^2 M_R^6}{128\pi^3 v^2 m_h^4} \quad (\text{A.2})$$

leading to a lifetime

$$\tau(\nu_R \rightarrow \nu_L f \bar{f}) \sim (1 \text{ s}) \times \left(\frac{10 \text{ GeV}}{M_R}\right)^6 \times \left(\frac{0.1 \text{ eV}}{m_\nu}\right) \times \left(\frac{y_b}{y_{\text{SM}}}\right)^2, \quad (\text{A.3})$$

where we have normalized the Yukawa coupling y_{SM} to the b -quark Yukawa coupling. If $M_R \gtrsim 2m_b$, we expect ν_R to decay predominantly a $b\bar{b}$ pair since this is the heaviest SM fermions that are kinematically available for the 2-body decay. If M_R is slightly less than the $2m_b$ threshold, decays to $c\bar{c}$ and $\tau^+\tau^-$ would be present, with y_{SM} slightly smaller than y_b .

In any case, the above estimate demonstrates that for $M_R \lesssim 10 \text{ GeV}$, ν_R are comparatively long-lived and can disrupt BBN light element abundance predictions due to the electromagnetic energy deposition [168]. Given that the width, equation (A.2), depends on the 6th power of M_R , one only needs slightly larger masses, $M_R \gtrsim 20 \text{ GeV}$, to cause ν_R to decay sufficiently fast to completely avoid BBN constraints.

This leads to two possibilities in the Majorana scenario:

If ν_R was in thermal equilibrium in the early Universe, $M_R \gtrsim 20 \text{ GeV}$ is required to avoid BBN constraints, and thus $v_X \gtrsim (20 \text{ GeV})/y_M$. If X^μ acquires *all* of its mass from just the ϕ_X vev, then m_X is determined once g_X is specified, specifically, $m_X = 2g_X v_X$. The scalar Higgs sector of $U(1)_{B-L}$ need not be minimal. There could be other scalars with $B-L$ charge that differ ϕ_X , i.e., $\phi_{X'}$ with $q_{X'} \neq \pm 2$. These do not lead to contributions to the

Majorana masses, but will lead to an additional contribution to the X^μ gauge boson mass, $m_X^2 = g_X^2 (4v_X^2 + q_X^2 v_{X'}^2)$. Hence, we see that the minimal case $m_X = 2g_X v_X$ is a *lower* bound on m_X for a generic $U(1)_{B-L}$ breaking sector. Said directly, the bound $M_R \gtrsim 20$ GeV implies

$$g_X < \frac{m_X}{2v_X} \lesssim 2.5 \times 10^{-5} \frac{m_X}{1 \text{ MeV}} \quad (\text{if } \nu_R \text{ in early thermal equilibrium}). \quad (\text{A.4})$$

On the other hand, it could be that ν_R was never in thermal equilibrium in the early universe. In this case, no population of ν_R 's were generated, and there is no bound on g_X from ν_R decay.

B Finite Temperature Effects

In the SM, finite temperature effects [39, 60, 89] result in an $\mathcal{O}(0.01)$ correction to N_{eff} . One example is the finite shift in the photon's propagator due its self-energy $\Pi_{\mu\nu}$ in presence of an e^+e^- background. This shift generates a complex effective mass for the photon and modifies the dispersion relation of the longitudinal and transverse spin polarizations of the photon. To $\mathcal{O}(\alpha)$, a simplified version of the effective masses is

$$m_\gamma^2 = \begin{cases} 4\pi\alpha(n_e/m_e) & (T \ll m_e) \\ \frac{2}{3}\pi\alpha T^2 & (T \gg m_e). \end{cases} \quad (\text{B.1})$$

A similar story generates an effective mass for electrons

$$m_{e,\text{eff}}^2(T) \approx m_{e,0}^2 + \pi\alpha T^2. \quad (\text{B.2})$$

Note that $m_\gamma(T) < 2m_{e,\text{eff}}(T)$ and hence photon decay to e^+e^- pair is always kinematically forbidden.

Finite temperature correction to early universe dynamics with an additional hidden photon (which we label X for convenience) has also been explored in [169–175] and most relevant to our discussion here are [54, 90, 99, 176]. We will summarize this discussion and use the results to calculate the contribution of finite temperature effects in our model. In what follows, we only take the transverse part of photon polarization tensor, since it was shown in [54] that the longitudinal part of the photon polarization tensor does not significantly contribute to the finite temperature effects.

Following [99], for a given interaction $a\bar{a} \rightarrow X$, one can write the additional interaction $a\bar{a} \rightarrow \gamma \rightarrow X$, where $\gamma \rightarrow X$ is the contribution of all allowed fermion loops in medium. In vacuum, such interactions are loop-suppressed and are negligible. However, in a medium with finite temperature/density, these interactions are important and can, in some cases, dominate the rate [96, 97, 99, 177–179]. The $a\bar{a} \rightarrow \gamma \rightarrow X$ diagram is proportional to

$$e \frac{-i}{k^2 - \Pi_{\gamma-(f)-\gamma}} i\Pi_{\gamma-(f)-X}, \quad (\text{B.3})$$

where e is the electromagnetic coupling, the second piece is the in-medium photon propagator, and the third is the induced $\gamma-X$ mixing in medium. Assuming the two polarization tensors

have the same fermion loops, then $\Pi_{\gamma-(f)-X} = (g_X/e)\Pi_{\gamma-(f)-\gamma}$. The sum of the two diagrams is now given by

$$(a\bar{a} \rightarrow X) + (a\bar{a} \rightarrow \gamma \rightarrow X) \propto g_X \left(1 + \frac{\Pi_{\gamma\gamma}}{k^2 - \Pi_{\gamma\gamma}} \right) \quad (\text{B.4})$$

$$= g_X \frac{m_X^2}{m_X^2 - \Pi_{\gamma\gamma}}, \quad (\text{B.5})$$

and the modification to the coupling in medium can be written as,

$$g_{X,m}^2 = \frac{g_X^2 m_X^4}{|m_X^2 - \Pi|^2} = \frac{g_X^2 m_X^4}{(m_X^2 - m_\gamma^2)^2 + (\text{Im } \Pi)^2}, \quad (\text{B.6})$$

where $\text{Re } \Pi = m_\gamma^2$ in Eq. B.1. The imaginary part $\text{Im } \Pi$ [92] encodes the rate at which the photon's distribution approaches a thermal equilibrium,

$$\text{Im } \Pi = -\omega\Gamma \equiv -\omega[\Gamma_{\text{decay}}(\omega) + \Gamma_{\text{inverse}}(\omega)]. \quad (\text{B.7})$$

The imaginary part of the self-energy arises at two-loops and we generically have $\text{Im } \Pi \ll \text{Re } \Pi$. The effective coupling in Eq. B.6 can be discussed in three regimes; $m_\gamma(T) \gg m_X$, $m_X = m_\gamma(T_r)$, and $m_\gamma(T) \ll m_X$. The middle regime, $m_X = m_\gamma(T_r)$, is resonant. If the resonance occurs when the electrons are relativistic, $T \gg m_e$, the resonance temperature is

$$T_r = \sqrt{\frac{3}{2\pi\alpha}} m_X \approx 8m_X \quad (T \gg m_e). \quad (\text{B.8})$$

If the electrons are non-relativistic when the resonance occurs then $m_\gamma(T_r) \propto T_r^{3/2} e^{-m_e/T_r}$ as per Eq. B.1. The photon plasma mass is extremely sensitive to T and the resonance occurs around $T_r \sim 0.2m_e$ for a wide range of masses $m_X \sim (1 - 10^5 \text{ eV})$. We now discuss the regimes.

B.1 $m_\gamma(T) \ll m_X$

In this regime, the in-medium coupling $g_{X,m}$ reduces to its vacuum value g_X . We start by examining the entropy scaled number density $Y_X = n_X/s$ produced from forward interactions to X using only the vacuum coupling. We write the simplest Boltzmann equation

$$s\dot{Y}_X = \dot{n}_X + 3Hn_X = \sum_a \frac{3}{2\pi^2} \Gamma_{X \rightarrow a\bar{a}} m_X^2 T K_1(m_X/T). \quad (\text{B.9})$$

Here, we have assumed massless particles a with zero chemical potential and took the Maxwell-Boltzmann approximation for distributions in the collision term. Explicitly, the collision term includes $e^+e^- \rightarrow X$ and $\nu_i\bar{\nu}_i \rightarrow X$. The final Y_X^f from the following two forward interactions can be calculated

$$Y_X = \int_0^\infty dT \frac{\dot{Y}_X}{H(T)T} = \frac{3}{16\pi^2} \frac{g_X^2 m_X^4}{[Hs]_{T=m_X}} \times \begin{cases} (1) & (e^+e^- \rightarrow X) \\ (\frac{3}{2}) & (\nu\bar{\nu} \rightarrow X). \end{cases} \quad (\text{B.10})$$

In the next sections, we show that the finite temperature effects contributions to Y_X are negligible compared to Eq. B.10.

B.2 $m_\gamma(T) \gg m_X$

Here, the coupling $g_{X,m}$ is suppressed by a factor of m_X^2/m_γ^2 compared to its vacuum counterpart. However, this suppression occurs above resonance, $T_r > 8m_X$, where the X production rates are inefficient even in the vacuum case. In our Boltzmann evolution of X population and for small values of g_X , a negligible amount of X is produced in this temperature range. This makes this regime unimportant for our analysis, since this suppression would only decrease the amount of X produced. We ignore this regime in all subsequent discussion.

B.3 $m_\gamma(T) = m_X$ resonance

We now discuss the interactions that are allowed during the resonance and thus contribute to the resonant X production. *Importantly, the second diagram in Eq. B.4 does not exist for $\nu_i \bar{\nu}_i \rightarrow X$. The neutrino coalescence rate is not changed by finite temperature effects*⁸. Thus, Our treatment of neutrinos rates is complete and neutrinos do *not* contribute to the resonance. Furthermore, $e^+e^- \rightarrow X$ is kinematically allowed only for $m_X > 2m_{e,\text{eff}}$ or when

$$T \leq T_c = \sqrt{\frac{m_X^2 - 4m_{e,0}^2}{4\pi\alpha}} < T_r. \quad (\text{B.11})$$

Hence, e^+e^- coalescence also does *not* contribute to the resonance since the interaction is only allowed for temperatures strictly below T_{res} . This point is emphasized in [90], but missed in more recent literature [54, 176]. The contribution to the resonance in both our and the hidden photon case, comes from pair annihilation $e^+e^- \leftrightarrow \gamma X$ and semi-Compton $e\gamma \leftrightarrow eX$. The resonant production increases the initial value of ρ_X at the expense of energy density of the $e - \gamma$ plasma. The decay of X back into SM particles is unchanged. Explicitly, a larger initial ρ_X or a smaller initial $\rho_{\gamma-e}$ causes an increase the value of ΔN_{eff} .

In this case, the entropy scaled number density $Y_{X,\text{res}}$ produced from the resonance through the interaction $a + b \rightarrow X + c$ is [90],

$$s\dot{Y}_X = \int dn_a dn_b \tilde{\sigma}_{2 \rightarrow 2}(s) v_{\text{Mö}} \frac{g_X^2 m_X^4}{(m_X^2 - m_\gamma^2)^2 + (\text{Im}\Pi)^2}, \quad (\text{B.12})$$

where $\int dn_i = \int g_i dp_i^3 f_i / (2\pi)^3$, the $\tilde{\sigma} = \sigma / g_{X,m}^2$, and $v_{\text{Mö}}$ is the Moeller velocity. At resonance, expanding $m_\gamma^2 = m_X + (m_\gamma^2)'(T - T_r) + \dots$ and using the narrow width approximation,

$$\begin{aligned} \frac{g_X^2 m_X^4}{(m_X^2 - m_\gamma^2)^2 + (\text{Im}\Pi)^2} &= g_X^2 m_X^4 \frac{\pi}{(m_\gamma^2)' \text{Im}\Pi} \delta(T - T_r) \\ &= g_X^2 m_X^2 \frac{T}{j(T)} \frac{\pi}{\text{Im}\Pi} \delta(T - T_r), \end{aligned} \quad (\text{B.13})$$

where $j(T) \equiv \frac{T}{m_\gamma^2} (m_\gamma^2)'$ is a function defined in [90]. The integrals can be performed to obtain

$$\begin{aligned} Y_{X,\text{res}} &= \frac{2}{3\pi} g_X^2 m_X^2 \int_{m_X}^{\infty} d\omega \frac{1}{j(T_r) [Hs]_{T=T_r}} \frac{\sqrt{\omega^2 - m_X^2}}{e^{\omega/T_r} - 1} \\ &\approx \left(\frac{\pi}{9j(T_r)} \frac{m_X^3}{T_r^3} \right) \left(\frac{[\sqrt{g_* g_* S}]_{T=m_X}}{[\sqrt{g_* g_* S}]_{T=T_r}} \right) \frac{g_X^2 m_X^4}{[Hs]_{T=m_X}} \equiv \mathcal{AB} \frac{g_X^2 m_X^4}{[Hs]_{T=m_X}}, \end{aligned} \quad (\text{B.14})$$

⁸The transfer rate $\delta\rho_{X \rightarrow \nu_i \bar{\nu}_i} / \delta t$ is proportional to the distribution f_X . The only modification to this rate at a given temperature stems from modifications to f_X from other enhanced electron interactions. Nonetheless, The coupling g_X in the neutrino coalescence rate is unchanged.

where g_*, g_{*S} are the standard relativistic degrees of freedom in energy and entropy density. The factors \mathcal{A} and \mathcal{B} are defined as the terms in first and second set of parentheses respectively. In all cases, $T_r > m_X$ and $\mathcal{B} \leq 1$ and \mathcal{B} thus can only decrease the prefactor in Eq. B.14 in comparison to Eq. B.10. We will conservatively ignore \mathcal{B} in our argument as it depends on value of m_X . Furthermore, In a more detailed treatment of this derivation, m_γ^2 , and subsequently T_r and $j(T)$, have ω dependence. However, a numerical evaluation of the integral in Eq. B.14 taking this dependence into accounts does not significantly change the values of $Y_{X,\text{res}}$ discussed here.

B.4 Implications of the resonance on our results

For $m_X \gtrsim 2m_e$, the resonance occurs at $T_r \sim 8m_X$ where $j(T_r) = 2$. With these substitutions, the factor \mathcal{A} in Eq. B.14 is suppressed by $1/8^3$ and is $\mathcal{A} \sim \mathcal{O}(10^{-4})$. Since $e^+e^- \rightarrow X$ is active, comparing these values to $\mathcal{O}(10^{-2})$ prefactor in Eq. B.10 one finds that finite temperature effects contribute at most a few percent to Y_X .

For $m_X \ll m_e$, the resonance occurs around 30 – 200 keV for a wide range of masses $m_X \sim 1 - 10^4$ eV. Importantly, the resonance is the only active mechanism that permits energy from the $e^+e^-\gamma$ plasma to be transferred into X bosons. For example, for $m_X = 10$ keV, the resonance temperature is $T_r \approx 200$ keV and $j(T_r) \approx 4$ giving $\mathcal{A} \sim \mathcal{O}(10^{-5})$. For $m_X = 10$ eV, then $T_r \approx 40$ keV and $j(T_r) \approx 10$ giving $\mathcal{A} \sim \mathcal{O}(10^{-13})$. Consequently, when the resonance process dominates the contribution to ΔN_{eff} , the constraints on g_X become increasingly weaker at lower m_X mass, illustrated by the $\Delta N_{\text{eff}} = 0.4, 0.5$ contours in figure 5 and $\Delta N_{\text{eff}} = 0.2$ and larger contours in figure 6.

References

- [1] J. Alexander et al., *Dark Sectors 2016 Workshop: Community Report*, 8, 2016, [1608.08632](#).
- [2] M. Battaglieri et al., *US Cosmic Visions: New Ideas in Dark Matter 2017: Community Report*, in *U.S. Cosmic Visions: New Ideas in Dark Matter*, 7, 2017, [1707.04591](#).
- [3] N. Arkani-Hamed, D. P. Finkbeiner, T. R. Slatyer and N. Weiner, *A Theory of Dark Matter*, *Phys. Rev. D* **79** (2009) 015014 [[0810.0713](#)].
- [4] M. Pospelov and A. Ritz, *Astrophysical Signatures of Secluded Dark Matter*, *Phys. Lett. B* **671** (2009) 391 [[0810.1502](#)].
- [5] M. Pospelov, *Secluded U(1) below the weak scale*, *Phys. Rev. D* **80** (2009) 095002 [[0811.1030](#)].
- [6] M. Fabbrichesi, E. Gabrielli and G. Lanfranchi, *The Dark Photon*, [2005.01515](#).
- [7] A. Davidson, *B – L as the fourth color within an SU(2)_L × U(1)_R × U(1) model*, *Phys. Rev. D* **20** (1979) 776.
- [8] R. E. Marshak and R. N. Mohapatra, *Quark - Lepton Symmetry and B-L as the U(1) Generator of the Electroweak Symmetry Group*, *Phys. Lett. B* **91** (1980) 222.
- [9] R. N. Mohapatra and R. E. Marshak, *Local B-L Symmetry of Electroweak Interactions, Majorana Neutrinos and Neutron Oscillations*, *Phys. Rev. Lett.* **44** (1980) 1316.
- [10] C. Wetterich, *Neutrino Masses and the Scale of B-L Violation*, *Nucl. Phys. B* **187** (1981) 343.
- [11] P. Langacker, *The Physics of Heavy Z' Gauge Bosons*, *Rev. Mod. Phys.* **81** (2009) 1199 [[0801.1345](#)].
- [12] R. Harnik, J. Kopp and P. A. N. Machado, *Exploring nu Signals in Dark Matter Detectors*, *JCAP* **07** (2012) 026 [[1202.6073](#)].

- [13] J. Heeck, *Unbroken $B - L$ symmetry*, *Phys. Lett. B* **739** (2014) 256 [[1408.6845](#)].
- [14] M. Bauer, P. Foldenauer and J. Jaeckel, *Hunting All the Hidden Photons*, *JHEP* **07** (2018) 094 [[1803.05466](#)].
- [15] P. Ilten, Y. Soreq, M. Williams and W. Xue, *Serendipity in dark photon searches*, *JHEP* **06** (2018) 004 [[1801.04847](#)].
- [16] A. E. Nelson and N. Tetradis, *CONSTRAINTS ON A NEW VECTOR BOSON COUPLED TO BARYONS*, *Phys. Lett. B* **221** (1989) 80.
- [17] C. D. Carone and H. Murayama, *Possible light $U(1)$ gauge boson coupled to baryon number*, *Phys. Rev. Lett.* **74** (1995) 3122 [[hep-ph/9411256](#)].
- [18] P. Fileviez Perez and M. B. Wise, *Baryon and lepton number as local gauge symmetries*, *Phys. Rev. D* **82** (2010) 011901 [[1002.1754](#)].
- [19] R. Foot, *New Physics From Electric Charge Quantization?*, *Mod. Phys. Lett. A* **6** (1991) 527.
- [20] X. G. He, G. C. Joshi, H. Lew and R. R. Volkas, *NEW Z-prime PHENOMENOLOGY*, *Phys. Rev. D* **43** (1991) 22.
- [21] X.-G. He, G. C. Joshi, H. Lew and R. R. Volkas, *Simplest Z-prime model*, *Phys. Rev. D* **44** (1991) 2118.
- [22] M. Escudero, D. Hooper, G. Krnjaic and M. Pierre, *Cosmology with A Very Light $L_\mu - L_\tau$ Gauge Boson*, *JHEP* **03** (2019) 071 [[1901.02010](#)].
- [23] J. A. Dror, *Discovering leptonic forces using nonconserved currents*, *Phys. Rev. D* **101** (2020) 095013 [[2004.04750](#)].
- [24] N. Okada, S. Okada and Q. Shafi, *Light Z' and dark matter from $U(1)_X$ gauge symmetry*, *Phys. Lett. B* **810** (2020) 135845 [[2003.02667](#)].
- [25] PLANCK collaboration, N. Aghanim et al., *Planck 2018 results. I. Overview and the cosmological legacy of Planck*, *Astron. Astrophys.* **641** (2020) A1 [[1807.06205](#)].
- [26] PLANCK collaboration, N. Aghanim et al., *Planck 2018 results. VI. Cosmological parameters*, *Astron. Astrophys.* **641** (2020) A6 [[1807.06209](#)].
- [27] R. H. Cyburt, B. D. Fields, K. A. Olive and T.-H. Yeh, *Big Bang Nucleosynthesis: 2015*, *Rev. Mod. Phys.* **88** (2016) 015004 [[1505.01076](#)].
- [28] T.-H. Yeh, K. A. Olive and B. D. Fields, *The impact of new $d(p, \gamma)3$ rates on Big Bang Nucleosynthesis*, *JCAP* **03** (2021) 046 [[2011.13874](#)].
- [29] T.-H. Yeh, J. Shelton, K. A. Olive and B. D. Fields, *Probing physics beyond the standard model: limits from BBN and the CMB independently and combined*, *JCAP* **10** (2022) 046 [[2207.13133](#)].
- [30] PARTICLE DATA GROUP collaboration, R. L. Workman et al., *Review of Particle Physics*, *PTEP* **2022** (2022) 083C01.
- [31] P. F. de Salas and S. Pastor, *Relic neutrino decoupling with flavour oscillations revisited*, *JCAP* **07** (2016) 051 [[1606.06986](#)].
- [32] G. Mangano, G. Miele, S. Pastor, T. Pinto, O. Pisanti and P. D. Serpico, *Relic neutrino decoupling including flavor oscillations*, *Nucl. Phys. B* **729** (2005) 221 [[hep-ph/0506164](#)].
- [33] A. D. Dolgov, *Neutrinos in cosmology*, *Phys. Rept.* **370** (2002) 333 [[hep-ph/0202122](#)].
- [34] D. A. Dicus, E. W. Kolb, A. M. Gleeson, E. C. G. Sudarshan, V. L. Teplitz and M. S. Turner, *Primordial Nucleosynthesis Including Radiative, Coulomb, and Finite Temperature Corrections to Weak Rates*, *Phys. Rev. D* **26** (1982) 2694.

- [35] S. Hannestad and J. Madsen, *Neutrino decoupling in the early universe*, *Phys. Rev. D* **52** (1995) 1764 [[astro-ph/9506015](#)].
- [36] S. Dodelson and M. S. Turner, *Nonequilibrium neutrino statistical mechanics in the expanding universe*, *Phys. Rev. D* **46** (1992) 3372.
- [37] A. D. Dolgov, S. H. Hansen and D. V. Semikoz, *Nonequilibrium corrections to the spectra of massless neutrinos in the early universe*, *Nucl. Phys. B* **503** (1997) 426 [[hep-ph/9703315](#)].
- [38] S. Esposito, G. Miele, S. Pastor, M. Peloso and O. Pisanti, *Nonequilibrium spectra of degenerate relic neutrinos*, *Nucl. Phys. B* **590** (2000) 539 [[astro-ph/0005573](#)].
- [39] G. Mangano, G. Miele, S. Pastor and M. Peloso, *A Precision calculation of the effective number of cosmological neutrinos*, *Phys. Lett. B* **534** (2002) 8 [[astro-ph/0111408](#)].
- [40] J. Birrell, C.-T. Yang and J. Rafelski, *Relic Neutrino Freeze-out: Dependence on Natural Constants*, *Nucl. Phys. B* **890** (2014) 481 [[1406.1759](#)].
- [41] E. Grohs, G. M. Fuller, C. T. Kishimoto, M. W. Paris and A. Vlasenko, *Neutrino energy transport in weak decoupling and big bang nucleosynthesis*, *Phys. Rev. D* **93** (2016) 083522 [[1512.02205](#)].
- [42] M. Cielo, M. Escudero, G. Mangano and O. Pisanti, *Neff in the Standard Model at NLO is 3.043*, [2306.05460](#).
- [43] K. Akita and M. Yamaguchi, *A precision calculation of relic neutrino decoupling*, *JCAP* **08** (2020) 012 [[2005.07047](#)].
- [44] J. Froustey, C. Pitrou and M. C. Volpe, *Neutrino decoupling including flavour oscillations and primordial nucleosynthesis*, *JCAP* **12** (2020) 015 [[2008.01074](#)].
- [45] J. J. Bennett, G. Buldgen, P. F. De Salas, M. Drewes, S. Gariazzo, S. Pastor et al., *Towards a precision calculation of N_{eff} in the Standard Model II: Neutrino decoupling in the presence of flavour oscillations and finite-temperature QED*, *JCAP* **04** (2021) 073 [[2012.02726](#)].
- [46] S. Sarkar, *Big bang nucleosynthesis and physics beyond the standard model*, *Rept. Prog. Phys.* **59** (1996) 1493 [[hep-ph/9602260](#)].
- [47] F. Iocco, G. Mangano, G. Miele, O. Pisanti and P. D. Serpico, *Primordial Nucleosynthesis: from precision cosmology to fundamental physics*, *Phys. Rept.* **472** (2009) 1 [[0809.0631](#)].
- [48] M. Pospelov and J. Pradler, *Big Bang Nucleosynthesis as a Probe of New Physics*, *Ann. Rev. Nucl. Part. Sci.* **60** (2010) 539 [[1011.1054](#)].
- [49] M. Blennow, E. Fernandez-Martinez, O. Mena, J. Redondo and P. Serra, *Asymmetric Dark Matter and Dark Radiation*, *JCAP* **07** (2012) 022 [[1203.5803](#)].
- [50] C. Boehm, M. J. Dolan and C. McCabe, *Increasing N_{eff} with particles in thermal equilibrium with neutrinos*, *JCAP* **12** (2012) 027 [[1207.0497](#)].
- [51] C. Boehm, M. J. Dolan and C. McCabe, *A Lower Bound on the Mass of Cold Thermal Dark Matter from Planck*, *JCAP* **08** (2013) 041 [[1303.6270](#)].
- [52] C. Brust, D. E. Kaplan and M. T. Walters, *New Light Species and the CMB*, *JHEP* **12** (2013) 058 [[1303.5379](#)].
- [53] H. Vogel and J. Redondo, *Dark Radiation constraints on minicharged particles in models with a hidden photon*, *JCAP* **02** (2014) 029 [[1311.2600](#)].
- [54] A. Fradette, M. Pospelov, J. Pradler and A. Ritz, *Cosmological Constraints on Very Dark Photons*, *Phys. Rev. D* **90** (2014) 035022 [[1407.0993](#)].
- [55] K. M. Nollett and G. Steigman, *BBN And The CMB Constrain Neutrino Coupled Light WIMPs*, *Phys. Rev. D* **91** (2015) 083505 [[1411.6005](#)].

- [56] M. A. Buen-Abad, G. Marques-Tavares and M. Schmaltz, *Non-Abelian dark matter and dark radiation*, *Phys. Rev. D* **92** (2015) 023531 [[1505.03542](#)].
- [57] Z. Chacko, Y. Cui, S. Hong and T. Okui, *Hidden dark matter sector, dark radiation, and the CMB*, *Phys. Rev. D* **92** (2015) 055033 [[1505.04192](#)].
- [58] R. J. Wilkinson, A. C. Vincent, C. Boehm and C. McCabe, *Ruling out the light weakly interacting massive particle explanation of the Galactic 511 keV line*, *Phys. Rev. D* **94** (2016) 103525 [[1602.01114](#)].
- [59] G.-y. Huang, T. Ohlsson and S. Zhou, *Observational Constraints on Secret Neutrino Interactions from Big Bang Nucleosynthesis*, *Phys. Rev. D* **97** (2018) 075009 [[1712.04792](#)].
- [60] M. Escudero, *Neutrino decoupling beyond the Standard Model: CMB constraints on the Dark Matter mass with a fast and precise N_{eff} evaluation*, *JCAP* **02** (2019) 007 [[1812.05605](#)].
- [61] K. N. Abazajian and J. Heeck, *Observing Dirac neutrinos in the cosmic microwave background*, *Phys. Rev. D* **100** (2019) 075027 [[1908.03286](#)].
- [62] M. Ibe, S. Kobayashi, Y. Nakayama and S. Shirai, *Cosmological constraint on dark photon from N_{eff}* , *JHEP* **04** (2020) 009 [[1912.12152](#)].
- [63] M. Escudero Abenza, *Precision Early Universe Thermodynamics Made Simple: N_{eff} and Neutrino Decoupling in the Standard Model and Beyond*, *JCAP* **05** (2020) 048 [[2001.04466](#)].
- [64] J. Coffey, L. Forestell, D. E. Morrissey and G. White, *Cosmological Bounds on sub-GeV Dark Vector Bosons from Electromagnetic Energy Injection*, *JHEP* **07** (2020) 179 [[2003.02273](#)].
- [65] X. Luo, W. Rodejohann and X.-J. Xu, *Dirac neutrinos and N_{eff}* , *JCAP* **06** (2020) 058 [[2005.01629](#)].
- [66] X. Luo, W. Rodejohann and X.-J. Xu, *Dirac neutrinos and N_{eff} . Part II. The freeze-in case*, *JCAP* **03** (2021) 082 [[2011.13059](#)].
- [67] P. Adshead, P. Ralegankar and J. Shelton, *Dark radiation constraints on portal interactions with hidden sectors*, *JCAP* **09** (2022) 056 [[2206.13530](#)].
- [68] S. Eijima, O. Seto and T. Shimomura, *Revisiting sterile neutrino dark matter in gauged $U(1)_{B-L}$ model*, *Phys. Rev. D* **106** (2022) 103513 [[2207.01775](#)].
- [69] S. Sandner, M. Escudero and S. J. Witte, *Precision CMB constraints on eV-scale bosons coupled to neutrinos*, [2305.01692](#).
- [70] L. J. Hall, K. Jedamzik, J. March-Russell and S. M. West, *Freeze-In Production of FIMP Dark Matter*, *JHEP* **03** (2010) 080 [[0911.1120](#)].
- [71] M. Bordag, U. Mohideen and V. M. Mostepanenko, *New developments in the Casimir effect*, *Phys. Rept.* **353** (2001) 1 [[quant-ph/0106045](#)].
- [72] M. Bordag, G. L. Klimchitskaya, U. Mohideen and V. M. Mostepanenko, *Advances in the Casimir effect*, vol. 145. Oxford University Press, 2009.
- [73] E. G. Adelberger, B. R. Heckel, S. A. Hoedl, C. D. Hoyle, D. J. Kapner and A. Upadhye, *Particle Physics Implications of a Recent Test of the Gravitational Inverse Square Law*, *Phys. Rev. Lett.* **98** (2007) 131104 [[hep-ph/0611223](#)].
- [74] E. G. Adelberger, J. H. Gundlach, B. R. Heckel, S. Hoedl and S. Schlamminger, *Torsion balance experiments: A low-energy frontier of particle physics*, *Prog. Part. Nucl. Phys.* **62** (2009) 102.
- [75] S. Knapen, T. Lin and K. M. Zurek, *Light Dark Matter: Models and Constraints*, *Phys. Rev. D* **96** (2017) 115021 [[1709.07882](#)].
- [76] M. Kawasaki, K. Kohri and T. Moroi, *Big-Bang nucleosynthesis and hadronic decay of long-lived massive particles*, *Phys. Rev. D* **71** (2005) 083502 [[astro-ph/0408426](#)].

- [77] T. Kanzaki, M. Kawasaki, K. Kohri and T. Moroi, *Cosmological Constraints on Neutrino Injection*, *Phys. Rev. D* **76** (2007) 105017 [[0705.1200](#)].
- [78] M. Kawasaki, K. Kohri, T. Moroi, K. Murai and H. Murayama, *Big-bang nucleosynthesis with sub-GeV massive decaying particles*, *JCAP* **12** (2020) 048 [[2006.14803](#)].
- [79] J. Berger, K. Jedamzik and D. G. E. Walker, *Cosmological Constraints on Decoupled Dark Photons and Dark Higgs*, *JCAP* **11** (2016) 032 [[1605.07195](#)].
- [80] M. E. Peskin and D. V. Schroeder, *An Introduction to quantum field theory*. Addison-Wesley, Reading, USA, 1995.
- [81] K. Abazajian et al., *CMB-S4 Science Case, Reference Design, and Project Plan*, [1907.04473](#).
- [82] G. D. Kribs, G. Lee and A. Martin, *Effective field theory of Stückelberg vector bosons*, *Phys. Rev. D* **106** (2022) 055020 [[2204.01755](#)].
- [83] J. Preskill, *Gauge anomalies in an effective field theory*, *Annals Phys.* **210** (1991) 323.
- [84] N. Craig, I. Garcia Garcia and G. D. Kribs, *The UV fate of anomalous U(1)s and the Swampland*, *JHEP* **11** (2020) 063 [[1912.10054](#)].
- [85] S. Weinberg, *Cosmology*. 2008.
- [86] L. C. Thomas, T. Dezen, E. B. Grohs and C. T. Kishimoto, *Electron-Positron Annihilation Freeze-Out in the Early Universe*, *Phys. Rev. D* **101** (2020) 063507 [[1910.14050](#)].
- [87] S. Hannestad, *Oscillation effects on neutrino decoupling in the early universe*, *Phys. Rev. D* **65** (2002) 083006 [[astro-ph/0111423](#)].
- [88] A. D. Dolgov, S. H. Hansen, S. Pastor, S. T. Petcov, G. G. Raffelt and D. V. Semikoz, *Cosmological bounds on neutrino degeneracy improved by flavor oscillations*, *Nucl. Phys. B* **632** (2002) 363 [[hep-ph/0201287](#)].
- [89] N. Fornengo, C. W. Kim and J. Song, *Finite temperature effects on the neutrino decoupling in the early universe*, *Phys. Rev. D* **56** (1997) 5123 [[hep-ph/9702324](#)].
- [90] J. Redondo and M. Postma, *Massive hidden photons as lukewarm dark matter*, *JCAP* **02** (2009) 005 [[0811.0326](#)].
- [91] E. Braaten and D. Segel, *Neutrino energy loss from the plasma process at all temperatures and densities*, *Phys. Rev. D* **48** (1993) 1478 [[hep-ph/9302213](#)].
- [92] H. A. Weldon, *Simple Rules for Discontinuities in Finite Temperature Field Theory*, *Phys. Rev. D* **28** (1983) 2007.
- [93] C. S. Shin and S. Yun, *Dark gauge boson production from neutron stars via nucleon-nucleon bremsstrahlung*, *JHEP* **02** (2022) 133 [[2110.03362](#)].
- [94] D. Croon, G. Elor, R. K. Leane and S. D. McDermott, *Supernova Muons: New Constraints on Z' Bosons, Axions and ALPs*, *JHEP* **01** (2021) 107 [[2006.13942](#)].
- [95] G. Raffelt and D. Seckel, *Bounds on Exotic Particle Interactions from SN 1987a*, *Phys. Rev. Lett.* **60** (1988) 1793.
- [96] J. H. Chang, R. Essig and S. D. McDermott, *Revisiting Supernova 1987A Constraints on Dark Photons*, *JHEP* **01** (2017) 107 [[1611.03864](#)].
- [97] E. Hardy and R. Lasenby, *Stellar cooling bounds on new light particles: plasma mixing effects*, *JHEP* **02** (2017) 033 [[1611.05852](#)].
- [98] H. An, M. Pospelov, J. Pradler and A. Ritz, *Direct Detection Constraints on Dark Photon Dark Matter*, *Phys. Lett. B* **747** (2015) 331 [[1412.8378](#)].
- [99] S.-P. Li and X.-J. Xu, *Production rates of dark photons and Z' in the Sun and stellar cooling bounds*, [2304.12907](#).

- [100] TEXONO collaboration, M. Deniz et al., *Measurement of $Nu(e)\text{-bar}$ -Electron Scattering Cross-Section with a CsI(Tl) Scintillating Crystal Array at the Kuo-Sheng Nuclear Power Reactor*, *Phys. Rev. D* **81** (2010) 072001 [[0911.1597](#)].
- [101] S. Bilmis, I. Turan, T. M. Aliev, M. Deniz, L. Singh and H. T. Wong, *Constraints on Dark Photon from Neutrino-Electron Scattering Experiments*, *Phys. Rev. D* **92** (2015) 033009 [[1502.07763](#)].
- [102] BOREXINO collaboration, M. Agostini et al., *First Simultaneous Precision Spectroscopy of pp , ${}^7\text{Be}$, and pep Solar Neutrinos with Borexino Phase-II*, *Phys. Rev. D* **100** (2019) 082004 [[1707.09279](#)].
- [103] M. Lindner, F. S. Queiroz, W. Rodejohann and X.-J. Xu, *Neutrino-electron scattering: general constraints on Z' and dark photon models*, *JHEP* **05** (2018) 098 [[1803.00060](#)].
- [104] COHERENT collaboration, D. Akimov et al., *First Measurement of Coherent Elastic Neutrino-Nucleus Scattering on Argon*, *Phys. Rev. Lett.* **126** (2021) 012002 [[2003.10630](#)].
- [105] COHERENT collaboration, D. Akimov et al., *Measurement of the Coherent Elastic Neutrino-Nucleus Scattering Cross Section on CsI by COHERENT*, *Phys. Rev. Lett.* **129** (2022) 081801 [[2110.07730](#)].
- [106] S. K. A., A. Majumdar, D. K. Papoulias, H. Prajapati and R. Srivastava, *Implications of first LZ and XENONnT results: A comparative study of neutrino properties and light mediators*, *Phys. Lett. B* **839** (2023) 137742 [[2208.06415](#)].
- [107] P. Coloma, P. Coloma, M. C. Gonzalez-Garcia, M. C. Gonzalez-Garcia, M. Maltoni, M. Maltoni et al., *Constraining new physics with Borexino Phase-II spectral data*, *JHEP* **07** (2022) 138 [[2204.03011](#)].
- [108] P. J. Fox, R. Harnik, J. Kopp and Y. Tsai, *LEP Shines Light on Dark Matter*, *Phys. Rev. D* **84** (2011) 014028 [[1103.0240](#)].
- [109] BABAR collaboration, J. P. Lees et al., *Measurement of the $e^+e^- \rightarrow \pi^+\pi^-\pi^0\pi^0$ cross section using initial-state radiation at BABAR*, *Phys. Rev. D* **96** (2017) 092009 [[1709.01171](#)].
- [110] NA64 collaboration, D. Banerjee et al., *Search for vector mediator of Dark Matter production in invisible decay mode*, *Phys. Rev. D* **97** (2018) 072002 [[1710.00971](#)].
- [111] NA62 collaboration, E. Cortina Gil et al., *Search for production of an invisible dark photon in π^0 decays*, *JHEP* **05** (2019) 182 [[1903.08767](#)].
- [112] BELLE-II collaboration, I. Adachi et al., *Search for an Invisibly Decaying Z' Boson at Belle II in $e^+e^- \rightarrow \mu^+\mu^-(e^\pm\mu^\mp)$ Plus Missing Energy Final States*, *Phys. Rev. Lett.* **124** (2020) 141801 [[1912.11276](#)].
- [113] G. Bernardi et al., *Search for Neutrino Decay*, *Phys. Lett. B* **166** (1986) 479.
- [114] CHARM collaboration, F. Bergsma et al., *Search for Axion Like Particle Production in 400-GeV Proton - Copper Interactions*, *Phys. Lett. B* **157** (1985) 458.
- [115] A. Konaka et al., *Search for Neutral Particles in Electron Beam Dump Experiment*, *Phys. Rev. Lett.* **57** (1986) 659.
- [116] E. M. Riordan et al., *A Search for Short Lived Axions in an Electron Beam Dump Experiment*, *Phys. Rev. Lett.* **59** (1987) 755.
- [117] J. D. Bjorken, S. Ecklund, W. R. Nelson, A. Abashian, C. Church, B. Lu et al., *Search for Neutral Metastable Penetrating Particles Produced in the SLAC Beam Dump*, *Phys. Rev. D* **38** (1988) 3375.
- [118] A. Bross, M. Crisler, S. H. Pordes, J. Volk, S. Errede and J. Wrbanek, *A Search for Shortlived Particles Produced in an Electron Beam Dump*, *Phys. Rev. Lett.* **67** (1991) 2942.

- [119] M. Davier and H. Nguyen Ngoc, *An Unambiguous Search for a Light Higgs Boson*, *Phys. Lett. B* **229** (1989) 150.
- [120] NOMAD collaboration, P. Astier et al., *Search for heavy neutrinos mixing with tau neutrinos*, *Phys. Lett. B* **506** (2001) 27 [[hep-ex/0101041](#)].
- [121] J. Blumlein and J. Brunner, *New Exclusion Limits for Dark Gauge Forces from Beam-Dump Data*, *Phys. Lett. B* **701** (2011) 155 [[1104.2747](#)].
- [122] S. N. Gninenko, *Stringent limits on the $\pi^0 \rightarrow \gamma X, X \rightarrow e + e^-$ decay from neutrino experiments and constraints on new light gauge bosons*, *Phys. Rev. D* **85** (2012) 055027 [[1112.5438](#)].
- [123] S. N. Gninenko, *Constraints on sub-GeV hidden sector gauge bosons from a search for heavy neutrino decays*, *Phys. Lett. B* **713** (2012) 244 [[1204.3583](#)].
- [124] BABAR collaboration, J. P. Lees et al., *Search for a Dark Photon in e^+e^- Collisions at BaBar*, *Phys. Rev. Lett.* **113** (2014) 201801 [[1406.2980](#)].
- [125] LHCb collaboration, R. Aaij et al., *Search for Dark Photons Produced in 13 TeV pp Collisions*, *Phys. Rev. Lett.* **120** (2018) 061801 [[1710.02867](#)].
- [126] A. Berlin, N. Blinov and S. W. Li, *Dark Sector Equilibration During Nucleosynthesis*, *Phys. Rev. D* **100** (2019) 015038 [[1904.04256](#)].
- [127] E. Aver, K. A. Olive and E. D. Skillman, *The effects of He I $\lambda 10830$ on helium abundance determinations*, *JCAP* **07** (2015) 011 [[1503.08146](#)].
- [128] A. G. Riess et al., *New Parallaxes of Galactic Cepheids from Spatially Scanning the Hubble Space Telescope: Implications for the Hubble Constant*, *Astrophys. J.* **855** (2018) 136 [[1801.01120](#)].
- [129] Z. Hou, R. Keisler, L. Knox, M. Millea and C. Reichardt, *How Massless Neutrinos Affect the Cosmic Microwave Background Damping Tail*, *Phys. Rev. D* **87** (2013) 083008 [[1104.2333](#)].
- [130] E. Aver, D. A. Berg, K. A. Olive, R. W. Pogge, J. J. Salzer and E. D. Skillman, *Improving helium abundance determinations with Leo P as a case study*, *JCAP* **03** (2021) 027 [[2010.04180](#)].
- [131] M. Valerdi, A. Peimbert, M. Peimbert and A. Sixtos, *Determination of the Primordial Helium Abundance Based on NGC 346, an H ii Region of the Small Magellanic Cloud*, *Astrophys. J.* **876** (2019) 98 [[1904.01594](#)].
- [132] V. Fernández, E. Terlevich, A. I. Díaz and R. Terlevich, *A Bayesian direct method implementation to fit emission line spectra: Application to the primordial He abundance determination*, *Mon. Not. Roy. Astron. Soc.* **487** (2019) 3221 [[1905.09215](#)].
- [133] O. A. Kurichin, P. A. Kislitsyn, V. V. Klimenko, S. A. Balashev and A. V. Ivanchik, *A new determination of the primordial helium abundance using the analyses of H II region spectra from SDSS*, *Mon. Not. Roy. Astron. Soc.* **502** (2021) 3045 [[2101.09127](#)].
- [134] T. Hsyu, R. J. Cooke, J. X. Prochaska and M. Bolte, *The PHLEK Survey: A New Determination of the Primordial Helium Abundance*, *Astrophys. J.* **896** (2020) 77 [[2005.12290](#)].
- [135] A. G. Riess et al., *A 2.4% Determination of the Local Value of the Hubble Constant*, *Astrophys. J.* **826** (2016) 56 [[1604.01424](#)].
- [136] A. G. Riess et al., *Milky Way Cepheid Standards for Measuring Cosmic Distances and Application to Gaia DR2: Implications for the Hubble Constant*, *Astrophys. J.* **861** (2018) 126 [[1804.10655](#)].
- [137] M. Pettini and R. Cooke, *A new, precise measurement of the primordial abundance of Deuterium*, *Mon. Not. Roy. Astron. Soc.* **425** (2012) 2477 [[1205.3785](#)].

- [138] R. Cooke, M. Pettini, R. A. Jorgenson, M. T. Murphy and C. C. Steidel, *Precision measures of the primordial abundance of deuterium*, *Astrophys. J.* **781** (2014) 31 [1308.3240].
- [139] S. Riemer-Sørensen, J. K. Webb, N. Crighton, V. Dumont, K. Ali, S. Kotuš et al., *A robust deuterium abundance; Re-measurement of the $z=3.256$ absorption system towards the quasar PKS1937-1009*, *Mon. Not. Roy. Astron. Soc.* **447** (2015) 2925 [1412.4043].
- [140] R. J. Cooke, M. Pettini, K. M. Nollett and R. Jorgenson, *The primordial deuterium abundance of the most metal-poor damped Ly α system*, *Astrophys. J.* **830** (2016) 148 [1607.03900].
- [141] S. A. Balashev, E. O. Zavarygin, A. V. Ivanchik, K. N. Telikova and D. A. Varshalovich, *The primordial deuterium abundance: subDLA system at $z_{\text{abs}} = 2.437$ towards the QSO J 1444+2919*, *Mon. Not. Roy. Astron. Soc.* **458** (2016) 2188 [1511.01797].
- [142] S. Riemer-Sørensen, S. Kotuš, J. K. Webb, K. Ali, V. Dumont, M. T. Murphy et al., *A precise deuterium abundance: remeasurement of the $z = 3.572$ absorption system towards the quasar PKS1937-101*, *Mon. Not. Roy. Astron. Soc.* **468** (2017) 3239 [1703.06656].
- [143] E. O. Zavarygin, J. K. Webb, S. Riemer-Sørensen and V. Dumont, *Primordial deuterium abundance at $z_{\text{abs}} = 2:504$ towards Q1009+2956*, *J. Phys. Conf. Ser.* **1038** (2018) 012012 [1801.04704].
- [144] R. J. Cooke, M. Pettini and C. C. Steidel, *One Percent Determination of the Primordial Deuterium Abundance*, *Astrophys. J.* **855** (2018) 102 [1710.11129].
- [145] SPT-3G collaboration, B. A. Benson et al., *SPT-3G: A Next-Generation Cosmic Microwave Background Polarization Experiment on the South Pole Telescope*, *Proc. SPIE Int. Soc. Opt. Eng.* **9153** (2014) 91531P [1407.2973].
- [146] CORE collaboration, E. Di Valentino et al., *Exploring cosmic origins with CORE: Cosmological parameters*, *JCAP* **04** (2018) 017 [1612.00021].
- [147] SIMONS OBSERVATORY collaboration, P. Ade et al., *The Simons Observatory: Science goals and forecasts*, *JCAP* **02** (2019) 056 [1808.07445].
- [148] NASA PICO collaboration, S. Hanany et al., *PICO: Probe of Inflation and Cosmic Origins*, **1902.10541**.
- [149] N. Sehgal et al., *CMB-HD: An Ultra-Deep, High-Resolution Millimeter-Wave Survey Over Half the Sky*, **1906.10134**.
- [150] R. Consiglio, P. F. de Salas, G. Mangano, G. Miele, S. Pastor and O. Pisanti, *PARthENoPE reloaded*, *Comput. Phys. Commun.* **233** (2018) 237 [1712.04378].
- [151] S. Gariazzo, P. F. de Salas, O. Pisanti and R. Consiglio, *PARthENoPE revolutions*, *Comput. Phys. Commun.* **271** (2022) 108205 [2103.05027].
- [152] A. Arbey, *AlterBBN: A program for calculating the BBN abundances of the elements in alternative cosmologies*, *Comput. Phys. Commun.* **183** (2012) 1822 [1106.1363].
- [153] A. Arbey, J. Auffinger, K. P. Hickerson and E. S. Jentsen, *AlterBBN v2: A public code for calculating Big-Bang nucleosynthesis constraints in alternative cosmologies*, *Comput. Phys. Commun.* **248** (2020) 106982 [1806.11095].
- [154] C. Pitrou, A. Coc, J.-P. Uzan and E. Vangioni, *Precision big bang nucleosynthesis with improved Helium-4 predictions*, *Phys. Rept.* **754** (2018) 1 [1801.08023].
- [155] A.-K. Burns, T. M. P. Tait and M. Valli, *PRyMordial: The First Three Minutes, Within and Beyond the Standard Model*, **2307.07061**.
- [156] G. Krnjaic, *Dark Radiation from Inflationary Fluctuations*, *Phys. Rev. D* **103** (2021) 123507 [2006.13224].
- [157] F.-Y. Cyr-Racine and K. Sigurdson, *Limits on Neutrino-Neutrino Scattering in the Early Universe*, *Phys. Rev. D* **90** (2014) 123533 [1306.1536].

- [158] S. Bashinsky and U. Seljak, *Neutrino perturbations in CMB anisotropy and matter clustering*, *Phys. Rev. D* **69** (2004) 083002 [[astro-ph/0310198](#)].
- [159] D. Baumann, D. Green, J. Meyers and B. Wallisch, *Phases of New Physics in the CMB*, *JCAP* **01** (2016) 007 [[1508.06342](#)].
- [160] G. Choi, C.-T. Chiang and M. LoVerde, *Probing Decoupling in Dark Sectors with the Cosmic Microwave Background*, *JCAP* **06** (2018) 044 [[1804.10180](#)].
- [161] T. Schwemberger and T.-T. Yu, *Detecting beyond the standard model interactions of solar neutrinos in low-threshold dark matter detectors*, *Phys. Rev. D* **106** (2022) 015002 [[2202.01254](#)].
- [162] K. Kaneta, Z. Kang and H.-S. Lee, *Right-handed neutrino dark matter under the $B - L$ gauge interaction*, *JHEP* **02** (2017) 031 [[1606.09317](#)].
- [163] A. Biswas and A. Gupta, *Freeze-in Production of Sterile Neutrino Dark Matter in $U(1)_{B-L}$ Model*, *JCAP* **09** (2016) 044 [[1607.01469](#)].
- [164] K. J. Kelly, M. Sen, W. Tangarife and Y. Zhang, *Origin of sterile neutrino dark matter via secret neutrino interactions with vector bosons*, *Phys. Rev. D* **101** (2020) 115031 [[2005.03681](#)].
- [165] A. Berlin and N. Blinov, *Thermal Dark Matter Below an MeV*, *Phys. Rev. Lett.* **120** (2018) 021801 [[1706.07046](#)].
- [166] A. Berlin and N. Blinov, *Thermal neutrino portal to sub-MeV dark matter*, *Phys. Rev. D* **99** (2019) 095030 [[1807.04282](#)].
- [167] S.-P. Li and X.-J. Xu, *N_{eff} constraints on light mediators coupled to neutrinos: the dilution-resistant effect*, [2307.13967](#).
- [168] K. Jedamzik, *Big bang nucleosynthesis constraints on hadronically and electromagnetically decaying relic neutral particles*, *Phys. Rev. D* **74** (2006) 103509 [[hep-ph/0604251](#)].
- [169] J. Jaeckel, J. Redondo and A. Ringwald, *Signatures of a hidden cosmic microwave background*, *Phys. Rev. Lett.* **101** (2008) 131801 [[0804.4157](#)].
- [170] A. Mirizzi, J. Redondo and G. Sigl, *Microwave Background Constraints on Mixing of Photons with Hidden Photons*, *JCAP* **03** (2009) 026 [[0901.0014](#)].
- [171] P. Arias, D. Cadamuro, M. Goodsell, J. Jaeckel, J. Redondo and A. Ringwald, *WISPy Cold Dark Matter*, *JCAP* **06** (2012) 013 [[1201.5902](#)].
- [172] S. D. McDermott and S. J. Witte, *Cosmological evolution of light dark photon dark matter*, *Phys. Rev. D* **101** (2020) 063030 [[1911.05086](#)].
- [173] S. J. Witte, S. Rosauero-Alcaraz, S. D. McDermott and V. Poulin, *Dark photon dark matter in the presence of inhomogeneous structure*, *JHEP* **06** (2020) 132 [[2003.13698](#)].
- [174] A. Caputo, H. Liu, S. Mishra-Sharma and J. T. Ruderman, *Modeling Dark Photon Oscillations in Our Inhomogeneous Universe*, *Phys. Rev. D* **102** (2020) 103533 [[2004.06733](#)].
- [175] A. Caputo, H. Liu, S. Mishra-Sharma and J. T. Ruderman, *Dark Photon Oscillations in Our Inhomogeneous Universe*, *Phys. Rev. Lett.* **125** (2020) 221303 [[2002.05165](#)].
- [176] J.-T. Li, G. M. Fuller and E. Grohs, *Probing dark photons in the early universe with big bang nucleosynthesis*, *JCAP* **12** (2020) 049 [[2009.14325](#)].
- [177] J. Redondo, *Helioscope Bounds on Hidden Sector Photons*, *JCAP* **07** (2008) 008 [[0801.1527](#)].
- [178] H. An, M. Pospelov and J. Pradler, *New stellar constraints on dark photons*, *Phys. Lett. B* **725** (2013) 190 [[1302.3884](#)].
- [179] J. Redondo and G. Raffelt, *Solar constraints on hidden photons re-visited*, *JCAP* **08** (2013) 034 [[1305.2920](#)].